Relaxed Arakawa–Schubert: A Parameterization of Moist Convection for General Circulation Models

SHRINIVAS MOORTHI

Universities Space Research Association, Laboratory for Atmospheres, NASA/Goddard Space Flight Center, Greenbelt, Maryland

MAX J. SUAREZ

Laboratory for Atmospheres, NASA/Goddard Space Flight Center, Greenbelt, Maryland

(Manuscript received 6 February 1991, in final form 25 September 1991)

ABSTRACT

A simple implementation of the Arakawa and Schubert (1974) cumulus parameterization is presented. The major simplification made is to "relax" the state toward equilibrium each time the parameterization is invoked, rather than requiring that the final state be balanced, as in the original Arakawa–Schubert implementation. This relaxed Arakawa–Schubert (RAS) scheme is evaluated in off-line tests using the Global Atmospheric Research Program (GARP) Atlantic Tropical Experiment (GATE) Phase III data. The results show that RAS is equivalent to the standard implementation of Arakawa–Schubert but is more economical and simpler to code. RAS also avoids the ill-posed problem that occurs in Arakawa–Schubert as a result of having to solve for a balanced state.

1. Introduction

Arakawa and Schubert (1974; hereafter AS) developed a parameterization of cumulus convection for use in general circulation models (GCMs). The details of the implementation of the Arakawa–Schubert parameterization used in the UCLA GCM are given in Lord et al. (1982; hereafter LCA). We will refer to the implementation in LCA as the "standard" implementation since it is widely used and closely follows the formulation in AS.

The purpose of this paper is to present a much simpler implementation of the fundamental ideas in AS. We will call this new version of the parameterization "*relaxed Arakawa–Schubert*" (RAS). Because it is very efficient, while producing results very close to those of the standard AS implementation, RAS should be useful to both climate and numerical weather prediction modelers that wish to use the Arakawa–Schubert parameterization. In all that follows, we will rely heavily on AS and will assume that the reader is reasonably familiar with their parameterization.

RAS makes two major simplifications of the standard AS implementation.

1) It modifies the entrainment relation to avoid the costly calculation that is necessary to find the entrainment parameter of clouds detraining at the GCM levels.

2) Rather than requiring that "quasi equilibrium" of the cloud ensemble, in the AS sense, be achieved each time the parameterization is invoked, it only "relaxes" the state toward equilibrium.

The first assumption is a major economy and could be easily incorporated in any AS implementation. It has been used in the past in non-GCM applications (Shukla 1978; Chao 1979; Moorthi and Arakawa 1985).

The second assumption is more subtle and involves both a computational and a conceptual simplification. In simplest terms, the idea may be likened to solving the equations of the AS adjustment problem (an integral equation with nonlinear constraints) using numerical iteration. Taking such a view, the path along which one approaches quasi equilibrium depends on the iteration method chosen, but is inconsequential to AS as long as the iteration is carried close to convergence at time intervals shorter than the time scales at which AS demands that quasi equilibrium hold.

The iteration method chosen in RAS considers one cloud type (i.e., clouds that detrain at one of the GCM layers) at a time and computes the cumulus mass flux that would be required to maintain the invariance of the work function if there were no other clouds present. It then allows a fraction of this mass flux to change the sounding and goes on to do the same thing for another cloud type, letting it feel the modified sounding. With

Corresponding author address: Dr. Shrinivas Moorthi, Code 910.3, Laboratory for Atmospheres, NASA/Goddard Space Flight Center, Greenbelt, MD 20771.

this procedure, each step is in the direction of a single-cloud equilibrium, but in the course of iteration, all cloud types affect one another by modifying the environment. In practice, we do the equivalent of performing this iteration by doing a few steps (cloud types) at each "dynamics" time step rather than by bringing the iteration close to convergence on less frequent "physics" time intervals. The relaxation parameters (i.e., the fraction of the mass flux allowed to affect the sounding at each step of the iteration) depends on the time step, on a prescribed time scale, which may be different for each cloud type, and on the frequency with which each cloud type is selected.

The next sections will describe this procedure in detail, but we can clarify this a bit more at this point by comparing it with the usual AS implementation used in GCMs. The closure assumption in AS is based on their observation that the rate of change of the cloud work function A is small on time scales of several hours. The parameterization thus requires that the rate of change of A due to cumulus clouds balances the rate of change due to all other processes. In the standard implementation, this is accomplished by requiring that the cloud effects restore the cloud work function for each cloud type to some prescribed value. Since quasi equilibrium is a statement about the rate of change of A, not A itself, this further assumes that A had been previously set at this value (by the previous call to the parameterization) and that the departure from this prescribed critical value represents the large-scale forcing. A critical value of the cloud work function thus has to be specified for each cloud type. LCA use the mean A distribution of the tropical atmosphere and argue that there is some universality to it.

In RAS, we also assume quasi equilibrium, but we do this by having each cloud act to relax the cloud work function to a prescribed value with a cloud-type–dependent time scale. The time scale is chosen to be shorter than that of the large-scale forcing, with which cloud effects are to be equilibrated, and longer than the interval at which each cloud is allowed to modify the sounding. Quasi equilibrium is then approximately obtained for slowly varying external forcing.

Section 2 describes the scheme in its continuous form (details of a discrete version are given in the Appendix). We start in section 2a with a description of the cloud model. From the cloud model, we obtain the thermodynamic state (moist static energy and total water) at all levels inside clouds characterized by a given entrainment parameter λ. From these results, all cloud properties are completely determined. In section 2b, we write the cloud work function used by AS and use the results of section 2a to express it in terms of grid-scale (GCM) variables only. In section 2c, we write the tendency of the grid-scale variables due to cumulus clouds. Since we will be relaxing one cloud type at a time, these grid-scale tendencies are written for each cloud type separately. Combining the results of sections 2b and 2c, we find in section 2d the cloud effect on the cloud work function per unit mass flux. Again, since we treat one cloud type at a time, this is much simpler than the standard implementation. The closure is a balance between large-scale and grid-scale effects on the cloud work function. Given the larger-scale effects, this is a relation for the cloud-base mass flux of each cloud type. As mentioned above, in AS this results in an integral equation subject to the condition that cloud-base mass fluxes be nonnegative. Section 2d also describes how we solve for the mass fluxes. Section 2e describes how the mass fluxes are used to relax toward equilibrium and section 2f discusses the parameterization's application to vertically discrete models.

Section 3 presents a discussion of how the adjustment takes place and compares RAS with the standard implementation. Section 4 presents a semiprognostic evaluation of the parameterization using the Global Atmospheric Research Program (GARP) Atlantic Tropical Experiment (GATE) Phase III data. A prognostic evaluation of the scheme is given in section 5, and the results are discussed in section 6.

2. The parameterization

In this section the salient features of the parameterization in its continuous form are described. A discrete version of the parameterization for use in GCMs is described in detail in the Appendix. The results presented in subsequent sections are based on that discrete formulation of the parameterization.

a. The cloud model

The cloud model used here is essentially the same as in AS, with certain simplifying assumptions. We assume, as in AS, that an ensemble of clouds can be subdivided into subensembles characterized by a single parameter, λ (the entrainment parameter), and that all clouds have their base at the same height z_B. The first major simplification introduced is to assume that the normalized mass flux for each cloud type is a linear function of height (instead of an exponential function, as in AS). Then

$$\frac{\partial \eta_\lambda(z)}{\partial z} = \lambda, \tag{1}$$

where $\eta_\lambda(z)$ is the normalized mass flux for cloud type λ at height z and

$$\eta_\lambda(z_B) = 1. \tag{2}$$

The linear increase with height of the mass entrainment implies that, for a given λ, there is less dilution of cloud air at upper levels and thus results in deeper clouds than when the AS formula is used (or, stated another way, clouds that detrain at a given level will have a smaller cloud work function).

The hydrostatic equation is used in the form

$$\frac{\partial z}{\partial P} = -\frac{c_p}{g}\theta, \tag{3}$$

where $P = (p/p_0)^{R/c_p}$, p is the pressure, R is the gas constant, c_p is the specific heat at constant pressure, g is the gravitational acceleration, θ is the potential temperature, and p_0 is a standard value of p taken as 1000 hPa. Using (3) in (1),

$$\frac{\partial \eta_\lambda(P)}{\partial P} = -\frac{c_p}{g}\theta\lambda \tag{4}$$

is obtained and can be integrated to give

$$\eta_\lambda(P) = 1 + \frac{c_p}{g}\lambda\int_P^{P_B}\theta dP, \tag{5}$$

where $P_B \equiv P(z_B)$.

Next, as in AS, the large-scale budgets of moist static energy and total water substance for each cloud type are written as

$$\frac{\partial}{\partial P}[\eta_\lambda(P)h^c_\lambda(P)] = \frac{\partial \eta_\lambda(P)}{\partial P}h(P) \tag{6}$$

and

$$\frac{\partial}{\partial P}\{\eta_\lambda(P)[q^c_\lambda(P) + l^c_\lambda(P)]\} = \frac{\partial \eta_\lambda(P)}{\partial P}q(P), \tag{7}$$

where $h^c_\lambda(P)$, $q^c_\lambda(P)$, and $l^c_\lambda(P)$ are the cloud moist static energy, specific humidity, and liquid water mixing ratio for cloud type λ at level P, respectively, and $h(P)$ and $q(P)$ are the moist static energy and specific humidity in the environment, respectively.

In (7), the terms representing the precipitation process have been neglected for simplicity. We assume that all liquid water is carried to the cloud top where part is precipitated and part is evaporated, depending on the cloud type. (The formulation that is currently used is given in the Appendix.) There is no need to specify the vertical distribution of the precipitation because virtual effects and liquid water loading are not included, and so we do not need to know the vertical distribution of liquid water within the cloud. A justification for neglecting liquid water loading was presented recently by Cheng and Arakawa (1990). Both effects [liquid water loading and precipitation effects in (7)] are neglected in order to simplify the development. However, it is emphasized that they can be included in RAS without any conceptual complications.

With these assumptions, the level of nonbuoyancy for each cloud type is the level at which the moist static energy within the cloud is equal to the saturation moist static energy of the environment. That is,

$$h^c_\lambda(P_D) = h^*(P_D), \tag{8}$$

where $P_D(\lambda)$ is the level of vanishing buoyancy for the cloud type λ and is assumed to be the detrainment level. Integrating (6) from P_B to P_D, we get

$$\eta_\lambda(P_D)h^c_\lambda(P_D) - h_B = -\frac{c_p}{g}\lambda\int_{P_B}^{P_D}\theta h(P)dP. \tag{9}$$

Combining (5) evaluated at P_D and (9), we can solve (8) directly for the value of λ corresponding to clouds that detrain at a given level P_D:

$$\lambda(P_D) = \frac{h_B - h^*(P_D)}{\left(\frac{c_p}{g}\right)\int_{P_D}^{P_B}\theta(P)[h^*(P_D) - h(P)]dP}. \tag{10}$$

Similarly, assuming

$$q^c_\lambda(P_D) = q^*(P_D) \tag{11}$$

(i.e., that the cloud air is saturated at the level of nonbuoyancy) and integrating (7) from P_D to P_B, the liquid water mixing ratio at the detrainment level, $l(P_D)$, can be calculated from

$$l(P_D) \equiv l^c_\lambda(P_D) = \frac{1}{\eta_\lambda(P_D)} \times\left[q(P_B) + \frac{c_p}{g}\lambda\int_{P_D}^{P_B}\theta q(P)dP\right] - q^*(P_D). \tag{12}$$

b. The cloud work function

Following AS and neglecting the effects of water vapor and liquid water on the buoyancy, the cloud work function is written as

$$A_\lambda = \int_{z_B}^{z_D}\frac{g}{c_p\overline{T(z)}}\eta_\lambda(z)[s^c_\lambda(z) - s(z)]dz, \tag{13}$$

where A_λ is the cloud work function for cloud type λ, $\overline{T(z)}$ is the temperature in the environment at height z, and $s^c_\lambda(z)$ and $s(z)$ are the cloud's and the environment's dry static energies, respectively. Using the hydrostatic equation (3), (13) may be rewritten as

$$A_\lambda = \int_{P_D}^{P_B}\eta_\lambda(P)\frac{[s^c_\lambda(P) - s(P)]}{P}dP. \tag{14}$$

The development is simplified by writing (14) in terms of the moist static energy. Approximating

$$s^c_\lambda(P) - s(P) \approx \frac{1}{1 + \gamma(P)}[h^c_\lambda(P) - h^*(P)], \tag{15}$$

where $\gamma(P) = (L/c_p)[dq^*(P)/dT]$, L is the latent heat of condensation of water vapor and h^* and q^* are the saturation moist static energy and the saturation specific humidity of the environment, (14) becomes

$$A_\lambda = \int_{P_D}^{P_B}\frac{\eta_\lambda(P)}{1 + \gamma(P)}\frac{[h^c_\lambda(P) - h^*(P)]}{P}dP, \tag{16}$$

which is the form used here.

c. Cumulus effects on the large-scale budgets

The rate of change of dry and moist static energies due to cumulus convection can be written in the form

$$\left(\frac{\partial s}{\partial t}\right)_c = gM_c\frac{\partial s}{\partial p} - gLD(P)l(P)[1 - r(P)] \quad (17)$$

and

$$\left(\frac{\partial h}{\partial t}\right)_c = gM_c\frac{\partial h}{\partial p} + gD(P)(h^* - h), \quad (18)$$

where $M_c(P)$ is the total cumulus mass flux per unit horizontal area at level P, $D(P)$ is the detrained mass per unit area and pressure, and $r(P)$ is the fraction of the detrained liquid water that is precipitated. The choice of $r(P)$ used in this study is discussed in the Appendix.

In AS, $M_c(P)$ involves contributions from all cloud types penetrating level P. Thus,

$$M_c(P) = \int_0^{\lambda(P)} \eta_\lambda(P)m_B(\lambda)d\lambda, \quad (19)$$

where $\lambda(P)$ is given by (10), and $m_B(\lambda)$ is the cloud-base mass flux per unit λ. The mass detrainment per unit area and unit pressure depth is

$$D(P) = \eta_\lambda(P)m_B(\lambda)\frac{d\lambda(P)}{dp}. \quad (20)$$

In our case, we divide the continuous spectrum of clouds into subensembles of finite $\Delta\lambda$ and consider the effects of each subensemble independently. Thus, for the ith spectral band, extending from $\lambda_i - \Delta\lambda_i$ to λ_i,

$$M_c^i(P) = \begin{cases} \int_{\lambda_i-\Delta\lambda_i}^{\lambda_i} \eta_\lambda(P)m_B(\lambda)d\lambda, & P_D(\lambda_i) \geq P, \\ \int_{\lambda_i-\Delta\lambda_i}^{\lambda(P)} \eta_\lambda(P)m_B(\lambda)d\lambda, & \\ \qquad P_D(\lambda_i) \geq P \geq P_D(\lambda_i - \Delta\lambda_i), & \\ 0, \quad \text{otherwise} \end{cases} \quad (21)$$

and

$$D^i(P) = \begin{cases} \eta_\lambda(P)m_B(\lambda)\dfrac{d\lambda}{dp}, & \\ \qquad P_D(\lambda_i) \geq P \geq P_D(\lambda_i - \Delta\lambda_i) & \\ 0, \quad \text{otherwise} \end{cases} \quad (22)$$

where $P_D(\lambda_i)$, the detrainment level of clouds with $\lambda = \lambda_i$, may be obtained by solving (10).

Considering small $\Delta\lambda_i$, it is assumed that $m_B(\lambda)$ is uniform over this interval. Taking $m_B(\lambda) = m_B(\lambda_i)$ and neglecting terms in $(\Delta\lambda_i)^2$,

$$M_c^i(P) = \begin{cases} \eta_{\lambda_i}(P)m_B(\lambda_i)\Delta\lambda_i, & P > P_D(\lambda_i), \\ \eta_{\lambda_i}(P)m_B(\lambda_i)[\lambda(P) - \lambda_i + \Delta\lambda_i], & \\ \qquad P_D(\lambda_i) \geq P \geq P_D(\lambda_i - \Delta\lambda_i), & \\ 0, \quad \text{otherwise.} \end{cases} \quad (23)$$

Similarly, approximating the $d\lambda/dp$ in (22) by $\Delta\lambda_i[p_D(\lambda_i) - p_D(\lambda_i - \Delta\lambda_i)]^{-1}$ we obtain:

$$D^i(P) = \begin{cases} \eta_{\lambda_i}(P)m_B(\lambda_i)\Delta\lambda_i[p_D(\lambda_i) - p_D(\lambda_i - \Delta\lambda_i)]^{-1}, & \\ \qquad \text{for} \quad P_D(\lambda_i) \geq P \geq P_D(\lambda_i - \Delta\lambda_i), & \\ 0, \quad \text{otherwise.} \end{cases} \quad (24)$$

Then (17) and (18) can be rewritten as

$$\left(\frac{\partial s}{\partial t}\right)_c = \Gamma_s(P)m_B(\lambda_i)\Delta\lambda_i, \quad (25)$$

and

$$\left(\frac{\partial h}{\partial t}\right)_c = \Gamma_h(P)m_B(\lambda_i)\Delta\lambda_i, \quad (26)$$

where

$$\Gamma_s(P) \equiv \begin{cases} g\eta_{\lambda_i}(P)\dfrac{\partial s}{\partial p} \quad \text{for} \quad p > p_D(\lambda_i), & \\ g\eta_{\lambda_i}(P)[\lambda(P) - \lambda_i + \Delta\lambda_i](\Delta\lambda_i)^{-1}\dfrac{\partial s}{\partial p} & \\ \quad + g\eta_{\lambda_i}(P)[p_D(\lambda_i) - p_D(\lambda_i - \Delta\lambda_i)]^{-1} & \\ \quad \times l_{\lambda_i}(P_D)L[1 - r(P_D)], \quad \text{for} & \\ \qquad p_D(\lambda_i) \geq p \geq p_D(\lambda_i - \Delta\lambda_i), & \\ 0, \quad \text{otherwise} \end{cases} \quad (27)$$

and

$$\Gamma_h(P) \equiv \begin{cases} g\eta_{\lambda_i}(P)\dfrac{\partial h}{\partial p}, \quad \text{for} \quad p > p_D(\lambda_i), & \\ g\eta_{\lambda_i}(P)[\lambda(P) - \lambda_i + \Delta\lambda_i](\Delta\lambda_i)^{-1}\dfrac{\partial h}{\partial p} & \\ \quad + g\eta_{\lambda_i}(P)[p_D(\lambda_i) - p_D(\lambda_i - \Delta\lambda_i)]^{-1} & \\ \quad \times [h^*(P_D) - h(P_D)], \quad \text{for} & \\ \qquad p_D(\lambda_i) \geq p \geq p_D(\lambda_i - \Delta\lambda_i), & \\ 0, \quad \text{otherwise.} \end{cases} \quad (28)$$

From (25) and (26), the rate of change of potential temperature and specific humidity (which are the prognostic variables of our GCM) due to the ith cloud subensemble can be written as

$$\left(\frac{\partial \theta}{\partial t}\right)_c = \frac{m_B(\lambda_i)\Delta\lambda_i}{c_pP}\Gamma_s(P), \quad (29)$$

and

$$\left(\frac{\partial q}{\partial t}\right)_c = \frac{1}{L} m_B(\lambda_i)\Delta\lambda_i[\Gamma_h(P) - \Gamma_s(P)]. \quad (30)$$

d. The mass-flux kernel and cloud-base mass flux

Following AS, the rate of change of cloud work function is expressed as

$$\frac{dA_\lambda}{dt} = \left(\frac{dA_\lambda}{dt}\right)_c + \left(\frac{dA_\lambda}{dt}\right)_{ls}, \quad (31)$$

where the subscripts c and ls denote the contributions from the cloud-scale and the large-scale processes, respectively. By differentiating (16) with respect to time and ignoring the time variation of the pressures at the cloud base and top, as well as the time dependence of θ in (5), an approximate relation for the rate of change of A_λ can be obtained in terms of the rate of change the of large-scale variables, h and s (or θ and q):

$$\frac{dA_\lambda}{dt} = \int_{P_D}^{P_B} \frac{dP}{P[1+\gamma(P)]} \times \left\{\frac{\partial h(P_B)}{\partial t} - [1+\gamma(P)]\frac{\partial s(P)}{\partial t} + \frac{c_p}{g}\lambda \times \int_P^{P_B} \theta\left(\frac{\partial h(P')}{\partial t} - [1+\gamma(P)]\frac{\partial s(P)}{\partial t}\right)dP'\right\}. \quad (32)$$

Here the approximate relation

$$\frac{\partial h^*(P)}{\partial t} \approx [1+\gamma(P)]\frac{\partial s(P)}{\partial t} \quad (33)$$

is also used. In AS, cloud-scale contributions were written in the form

$$\left(\frac{dA_\lambda}{dt}\right)_c = \int_0^{\lambda_{\max}} K_{\lambda,\lambda'} m_B(\lambda')d\lambda', \quad (34)$$

where the kernel $K_{\lambda,\lambda'}$ represents the rate of change of the cloud work function of cloud type λ per unit cloud-base mass flux of cloud type λ'. These are not direct cloud–cloud interactions, but indirect effects of the various cloud types on each other through their environment. For quasi equilibrium to hold for the cumulus ensemble as a whole, these interactions must occur quickly compared to changes in the large-scale forcing. The standard implementation assumes that they occur instantaneously, resulting in a quasi-static balance between the cloud ensemble and the large-scale forcing. It is this assumption that results in an ill-posed problem, with the possibility that either *no* mass-flux distribution can produce an exact balance for all clouds with positive buoyancy or that (most frequently) *multiple* distributions can satisfy an "overadjustment" problem (Silva-Dias and Schubert 1977; LCA) in which some of the possible cloud types are overstabilized by the effects of other cloud types.

The main assumption of RAS is that the interaction between clouds, represented by the off-diagonal terms of K in (34), occur over a short but finite time and that at any instant each cloud (and each cloud type) feels only the "current" environment. Cloud interactions are then taken into account over time. The ill posedness of the standard implementation is thus removed by solving an initial value problem that selects an (overadjusted) equilibrium distribution that depends on the time scales specified for the adjustment of the individual cloud types. Thus, considering the effects of a single subensemble on the cloud work function, (34) reduces to

$$K_{\lambda_i,\lambda_i} = \frac{1}{m_B(\lambda_i)\Delta\lambda_i}\left(\frac{dA_{\lambda_i}}{dt}\right)_c. \quad (35)$$

Then, from (32), using the cloud-scale tendencies of s and h from (25) and (26), the following approximate relation for K_{λ_i,λ_i} can be obtained:

$$K_{\lambda_i,\lambda_i} = \int_{P_D}^{P_B} \frac{dP}{P[1+\gamma(P)]} \times \left\langle \Gamma_h(P_B) - [1+\gamma(P)]\Gamma_s(P) + \frac{c_p}{g}\lambda_i \times \int_P^{P_B} \theta\{\Gamma_h(P') - [1+\gamma(P)]\Gamma_s(P)\}dP' \right\rangle. \quad (36)$$

The subensemble cloud-base mass flux $m_B(\lambda_i)\Delta\lambda_i$ is obtained by equating the large-scale and cloud-scale changes of A:

$$m_B(\lambda_i)\Delta\lambda_i = \begin{cases} -\left(\dfrac{dA_{\lambda_i}}{dt}\right)_{ls} K^{-1}_{\lambda_i,\lambda_i}, & \text{for } m_B(\lambda_i) > 0 \\ 0, & \text{otherwise.} \end{cases} \quad (37)$$

The large-scale forcing, $(dA_{\lambda_i}/dt)_{ls}$, can be computed approximately from (32) by using the rate of change of h and s (or θ and q) due to large-scale processes such as advection, radiation, surface fluxes, etc. An alternate way to calculate the large-scale forcing is to use the following approximation:

$$\left(\frac{dA_{\lambda_i}}{dt}\right)_{ls} = \frac{A_{\lambda_i}(t+\Delta t) - A_{\lambda_i}(t)}{\Delta t}, \quad (38)$$

where $A_{\lambda_i}(t+\Delta t)$ is the cloud work function calculated from the profiles of θ and q after they are modified by the large-scale processes over a time interval Δt. This is a good approximation as long as Δt is small. This method is used to evaluate the large-scale forcing in the semiprognostic study presented in section 4. Using (38) in GCMs would require evaluating and storing the work function for each cloud type after modification of the environment by cumulus clouds. The large-scale forcing in GCMs that use the AS scheme is usually evaluated by replacing $A_{\lambda_i}(t+\Delta t)$ in (38) by the value

of the cloud work function after modification of the environment by large-scale effects and using a cloud-type–dependent critical value of the work function instead of $A_{\lambda_i}(t)$ (see LCA). This approach is used in the sensitivity study presented in section 3 and in the prognostic study presented in section 5.

e. *Adjustment of the large-scale environment*

As discussed in the Introduction, only a fraction α_{λ_i} of the mass flux needed to fully adjust a single cloud type [given by (37)] is allowed to affect the large-scale environment (grid-scale variables) at each step [i.e., $\alpha_{\lambda_i} m_B(\lambda_i)$ replaces $m_B(\lambda_i)$ in (29) and (30)]. This fraction depends on the size of time step and on a prescribed adjustment time scale, which may be cloud type dependent. The adjustment time scale may be thought of as the time over which the cloud effects would reduce the cloud work function to its equilibrium value and is of the order of 10^3–10^4 s (AS). If τ_{λ_i} is the adjustment time scale for the cloud type λ_i, then α_{λ_i} is taken as $\Delta t/\tau_{\lambda_i}$. Some discussion on the sensitivity of the parameterization to the selection of α_{λ_i} (or the time scale τ_{λ_i}) will be presented in next two sections.

f. *Application to vertically discrete models*

The formulation presented thus far applies to vertically continuous soundings, although the cumulus spectrum has been discretized into a series of subensembles characterized by their entrainment parameter λ. To derive a vertically discrete version of the parameterization for use in GCMs, it is convenient to associate the subensembles with the cloud-top level rather than the entrainment parameter (Lord and Arakawa 1980; LCA). Considering each subensemble separately, we can obtain a parameterization for the discrete model analogous to the one presented above for the vertically continuous case. The details of the discrete version of the parameterization are given in the Appendix.

A consequence of exchanging λ and the cloud-top pressure is that λ then becomes a dependent variable, and one must include it's time variation in the calculation for the kernel (Schubert 1973; Hack et al. 1984; Kao and Ogura 1987). In LCA, the kernel elements are computed by differentiating A numerically, and therefore the variation of λ is implicitly included. Since RAS requires only the diagonal elements of the kernel, it is straightforward to compute these terms explicitly. This has been done in the Appendix, where the relevant terms are proportional to ϑ. The effect of neglecting these terms is discussed in the next section.

3. Results from sensitivity tests

In this section, some results from off-line experiments are presented that were performed to explore the sensitivity of the parameterization to the choice of the relaxation parameter and to study the way in which the adjustments occur for various cloud types. For this purpose, an observed sounding was taken and RAS was iterated under various assumptions until the cloud work function was adjusted below the critical values proposed by LCA. The sounding used for all results in this section is from the ECMWF analysis for 1200 UTC 15 December 1979 at (2°N, 65°E).

The computations were performed using a nine-layer model with σ ($=p/p_s$; p_s is the surface pressure) as the vertical coordinate. The top seven layers have a thickness of $\Delta\sigma = 0.125$. The bottom layer has $\Delta\sigma = 0.05$ and the layer above it has $\Delta\sigma = 0.075$. We assume that all cloud types have their bases at $\sigma = 0.95$ (assuming the bottom layer to be the mixed layer below cloud base). The initial vertical profiles of the moist static energy h and the saturation moist static energy h^* as represented on this grid are shown in Fig. 1. It is clear from these profiles that clouds may reach up to 200 hPa; in fact, for six of the eight possible cloud types, the cloud work function exceeded the critical value of LCA. The choice of the initial sounding is quite arbitrary, but is representative of soundings the GCM would encounter during initialization. Surprisingly, the resulting adjustment problem is not that different from what the parameterization typically deals with in the course of GCM simulation. To get some feeling for how far from adjustment this sounding is, its "large-scale forcing" (i.e., the excess of the cloud work function over the LCA critical value for each cloud type) is compared with forcings obtained from a GCM integration using the standard implementation called every 450 s. As might be expected, the forcing used here was well above the average produced by the GCM (2–3 times larger, depending on the cloud type) but well below the largest adjustments made during the GCM run (10%–15% of the GCM cases required greater ad-

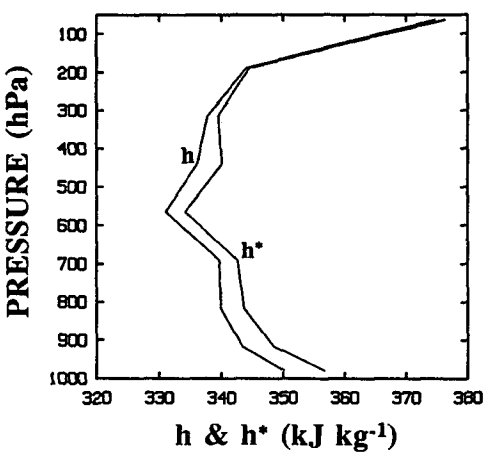

FIG. 1. The vertical profiles of moist static energy h and saturation moist static energy h^* at (2°N, 65°E) from the ECMWF analysis for 1200 UTC 15 December 1979.

justments). Even larger adjustments would have been required in the GCM if the parameterization had been called less frequently, as is customary. Therefore, this approach is considered an adequate and simple means of analyzing technical aspects of the behavior of the parameterization. More realistic tests are presented in sections 4 and 5.

a. Single-cloud experiments

First, the complete stabilization of individual clouds without cloud interactions is discussed. As mentioned before, when cloud types are characterized by their detrainment pressure level, rather than the entrainment parameter λ, the rate of change of λ enters the kernel [e.g., Eq. (A37)]. Therefore, we first consider the case for which this term is included [i.e., $\vartheta \neq 0$ in Eq. (A37)]. Figures 2a–d show the adjustments of the cloud work function, the total precipitation, the entrainment parameter, and the precipitation rate for the cloud type reaching the second highest layer (in this case no clouds detrain in the highest layer). We can see that the $\alpha_i = 1/4$ case adjusts the sounding in less than 16 iterations, while the $\alpha_i = 1/24$ case is still changing after 48 iterations.

Now the impact of neglecting the rate of change of the entrainment parameter λ [i.e., setting $\vartheta = 0$ in Eq. (A37)] on the adjustment process is discussed. Figures 3a–d show the cloud work function, the total precipitation, the entrainment parameter, and the precipitation rate for the cloud type detraining in the second model layer for the case with $\vartheta = 0$ (thick solid line for $\alpha_i = 1/4$ and thick dash-dot line for $\alpha_i = 1/24$) and for the case with $\vartheta \neq 0$ (thin solid line for $\alpha_i = 1/4$ and thin dash-dot line for $\alpha_i = 1/24$). We find from these figures that neglecting the rate of change of the entrainment parameter is roughly equivalent to a slight decrease in the relaxation parameter. This turns out to be true for all other cloud types, although the decrease of λ would have to be somewhat larger for the shallow cloud types. Since the inclusion of the rate of change of the entrainment parameter significantly complicates the calculation, and since the same result can be achieved by adjusting the relaxation parameter, ne-

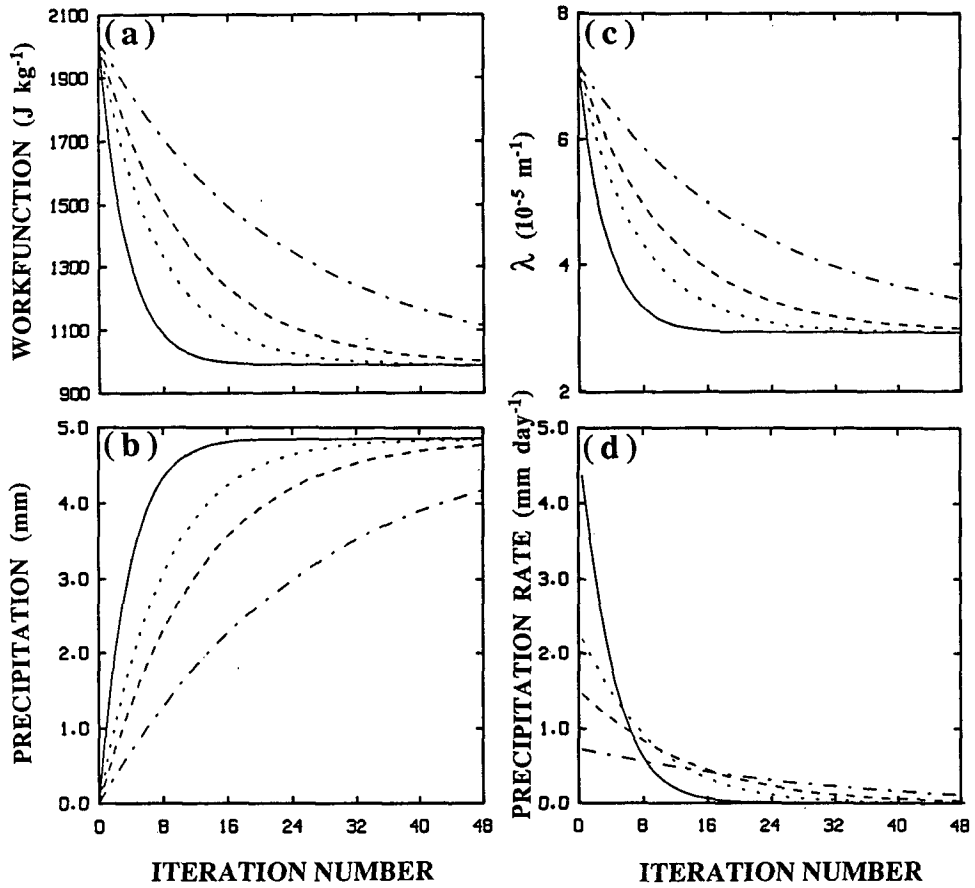

FIG. 2. Evolution of (a) the cloud work function (J kg^{-1}), (b) the precipitation (mm), (c) the entrainment parameter λ (10^{-5} m^{-1}), and (d) the precipitation rate (mm day^{-1}) as a function of iteration number for cloud type 2 in the single-cloud experiment. Results are shown for $\alpha = 1/4$ (solid curve), $\alpha = 1/8$ (dotted curve), $\alpha = 1/12$ (dashed curve), and $\alpha = 1/24$ (dash-dotted curve). The time rate of change of λ is included.

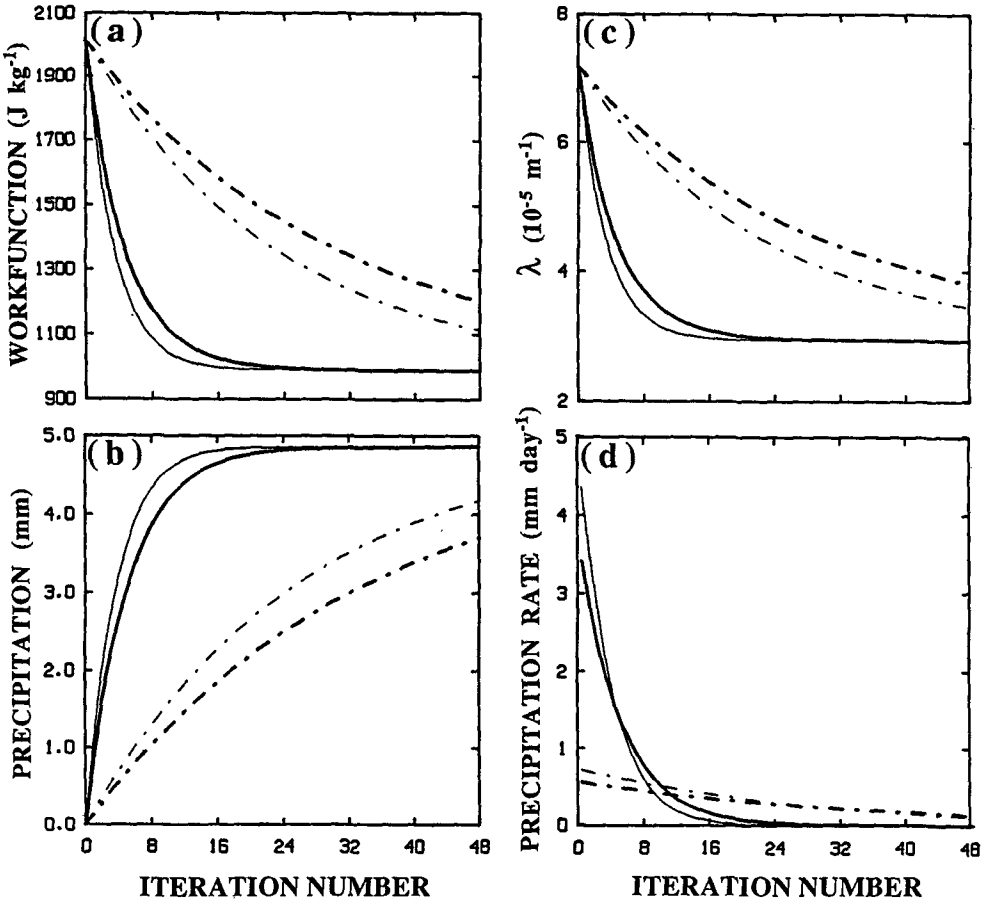

FIG. 3. The thin solid and thin dash-dot curves are the same as in Fig. 2. The thick solid and thick dash-dot curves are the corresponding curves when the time variation of λ is neglected.

glecting this effect is favorable when calculating the kernel elements. Thus, in all the results presented henceforth, the rate of change of λ at each step of the iteration has been ignored. This is not equivalent to ignoring this effect in the standard implementation because, as may be seen from Figs. 2c and 3c, λ changes considerably during the course of the adjustment. Thus, in RAS, most of the change in λ is taken into account over time, and neglecting the rate of change of λ terms at each step is a much more justifiable assumption than neglecting them in the standard implementation.

b. *Multicloud experiments*

Here the general case is considered for which many cloud types are invoked one after another (thus allowing for cloud interactions iteratively). This raises the question of the order in which cloud types are selected. Two approaches are considered: (i) to sequentially invoke all possible cloud types from the shallowest to the deepest for every iteration (i.e., cloud type 8 invoked first and cloud type 1 invoked last) or (ii) to invoke a fixed number of cloud types per iteration (or per time step in a prognostic model), but choosing them at random from a pool of all possible cloud types.

Invoking all cloud types sequentially works well when the number of vertical layers (and, therefore, the number of cloud types) is relatively small. However, as the vertical resolution increases, this would tend to favor strongly the clouds called first (the lowest in this case), since for thin layers adjacent clouds would have similar effects on the environment. In the extreme, the disturbed sounding could be stabilized even before all cloud types are invoked for the first time. To avoid such a possibility and to make the scheme independent of the number of vertical layers, the clouds may be selected randomly. The two methods are compared in the following discussion.

Figures 4a–d show the evolution of the cloud work function, precipitation, entrainment parameter, and precipitation rate of cloud type 2 (the same as in Fig. 2) for the sequential selection scheme using the same four values of the relaxation parameter as in Fig. 2. The time evolution of these parameters are smooth for all cloud types. The precipitation due to cloud type 2 is less than that in the corresponding single-cloud case

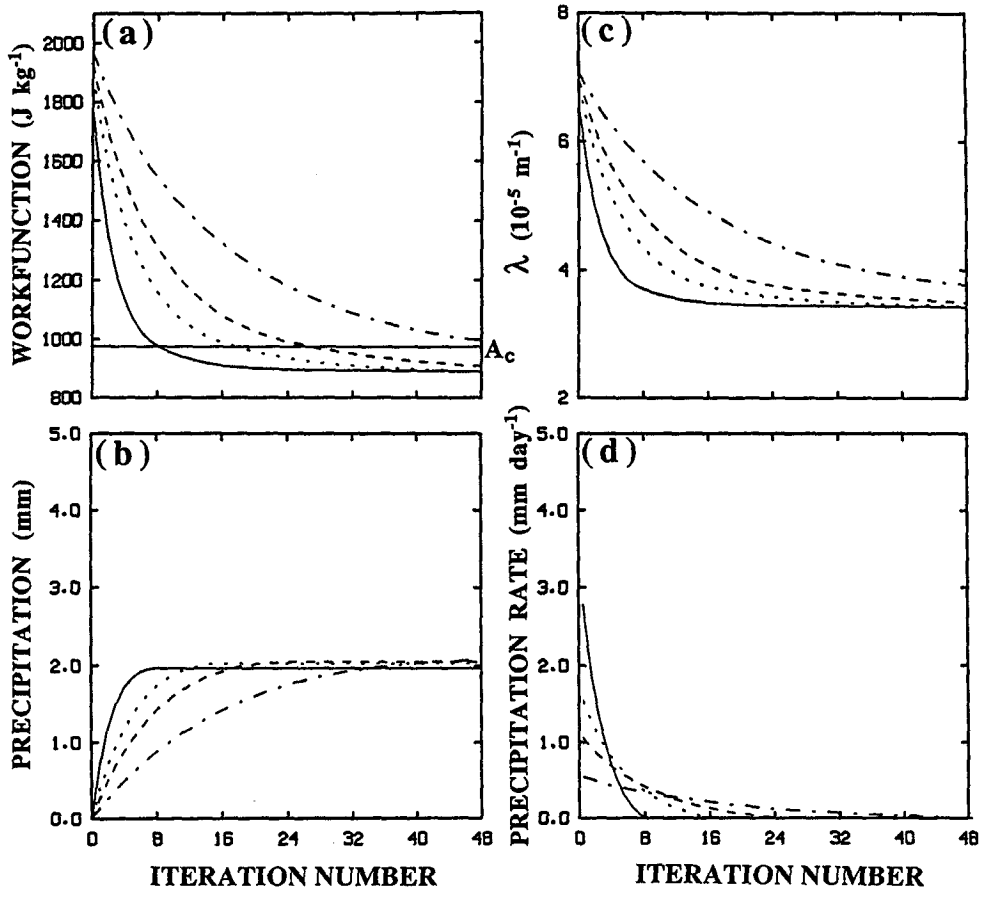

FIG. 4. Same as in Fig. 2, but for the multicloud experiment in which all cloud types are sequentially invoked from shallowest to deepest for each iteration.

(Fig. 2b), since other clouds are also active and precipitating. Notice that this cloud tends to overadjust slightly. For $\alpha = 1/4$, for example, the mass flux (as reflected in the precipitation rate in Fig. 4d) vanishes after eight iterations, when the work function reaches its critical value ($A_c = 987.5$ J kg^{-1}). The work function, however, continues to decrease due to the stabilizing effect of other, still active clouds. Finally, we note (by comparing Figs. 2c and 4c) that the cloud interactions tend to slightly lessen the amount of adjustment of the entrainment parameter.

The vertical profiles of the net heating (cooling) and moistening (drying) after 100 iterations (by which time all clouds are fully adjusted) are shown in Figs. 5a, b. It is encouraging that solutions for all relaxation parameters converge to practically the same values. This implies that cloud interactions are well accounted for, even when α is large. Making α large will allow us to maintain quasi equilibrium with fewer iterations.

To further illustrate how the multicloud solution is different from the single-cloud case, Figs. 6a–c present the values after 100 iterations of the cloud work function, the net precipitation, and the total mass exchange across the cloud base as a function of cloud type and relaxation parameter. The unshaded bars in these figures are for the single-cloud case with $\alpha_i = 1/4$, for which the sounding is fully adjusted. The multicloud cases are presented for all four values of α_i. We see that while the cloud work functions for the single-cloud cases converge exactly to their critical values, in the multicloud case they generally overadjust. However, it seems that this is not too sensitive to the value of the relaxation parameter.

The above set of experiments was repeated invoking cloud types randomly (selected from cloud types 2–8). The results were almost identical to those presented earlier and, therefore, are not shown. An experiment was also performed using random selection in which the relaxation parameter was varied linearly, from 1/4 for clouds detraining at 900 hPa to 1/12 for clouds detraining at 100 hPa. The results obtained in this case (not shown) were also very similar to those presented above.

c. *Comparison with the standard implementation*

In this section the aforementioned results using RAS will be compared with results obtained from the standard implementation. For this purpose, a vectorized version of the standard AS implementation (originally

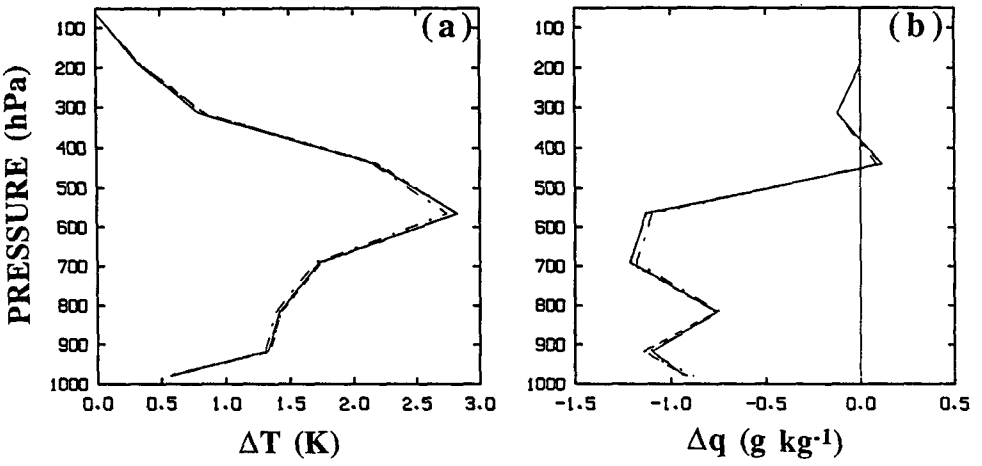

FIG. 5. Vertical distribution of temperature and moisture changes after full adjustment for the multicloud experiments of Fig. 4.

from UCLA GCM) adapted to a version of the Goddard Laboratory for Atmospheres (GLA) GCM (Sud et al. 1991) is used. Those cloud types for which $\lambda > 0$, $A > A_c$, and $K_{\lambda,\lambda} < 0$ with the initial sounding will be referred to as "possible clouds." In RAS, practically all possible clouds result in some mass flux, although, as shown in the previous section, some may be stabilized very quickly by the effects of other clouds. This is not true in the standard implementation, which tends to select one or two dominant clouds.

In the standard implementation, the cloud-base mass fluxes for all possible cloud types are obtained by solving a discretized mass-flux distribution equation using a linear programming method with overadjustment (for details, see LCA). The solution is obtained by using the simplex algorithm to minimize a linear combination of all the overadjustments. Because no physical justification has been given for specifying the weighting coefficients, the normalized overadjustments are usually assigned equal weights (LCA). Doing the adjustment in this way, many "possible" clouds are overadjusted and do not contribute to the cloud-base mass flux.

For the sounding shown in Fig. 1, the standard implementation found five possible cloud types (cloud types 2, 3, 4, 6, and 7), as compared with RAS, for which cloud type 8 was also possible. Thus, the determination of the cloud-base mass fluxes involved solving five equations for five nonnegative mass fluxes. For equal weighting of the overadjustments, the simplex procedure obtained a positive mass flux only for the deepest cloud (cloud type 2), with all other cloud types being overadjusted and having zero mass flux. The profiles of temperature and moisture changes for this solution are shown in Figs. 7a and 7b (solid circles). For comparison, those changes obtained by RAS when only cloud type 2 is allowed are also plotted (open circles). (The same profiles for the multicloud RAS solution were shown in Fig. 5.) We see that the temperature and moisture changes predicted by RAS are smaller than those of the standard implementation, although the vertical distributions are very similar. With RAS, the total mass exchange required for adjustment was 230 kg m^{-2}, whereas for the standard implementation it was 328 kg m^{-2}.

These differences are the result of several effects. The first is that, as mentioned above, the modification of the entrainment relation produces a smaller cloud work function in RAS than in the standard implementation. For this test, in which the cloud work function produced by an arbitrary observed sounding is taken and adjusted to the critical value, this implies a larger forcing in the standard implementation than in RAS. For cloud type 2, in fact, the forcing was ~37% larger. The systematic tendency of RAS to produce a smaller cloud work function can be easily remedied by using a correspondingly lower critical value than that obtained by LCA using the conventional formulation of the entrainment. However, since there is considerable uncertainty in the appropriate critical values (Cheng and Arakawa 1990; Sud et al. 1991), no attempt has been made to revise the LCA results.

For the single-cloud case, the mass flux is simply the ratio of the forcing to the diagonal kernel element as given by (37). RAS differs systematically from the standard implementation in the kernel as well as in the forcing. In the kernel, however, two competing effects are important. The first is again due to the modified entrainment relation, which produces a larger λ and thus a larger kernel [Eq. (36)]. Note that this effect is of the same sense as the λ effect on the forcing: it decreases the mass flux produced by RAS. For the cloud type 2 and the sounding being discussed, the diagonal kernel element obtained with the RAS cloud model was 30% larger than the one obtained with the standard cloud model. The second effect is that for the standard implementation, the kernel is obtained as a linearization about the initial, unadjusted profile. RAS

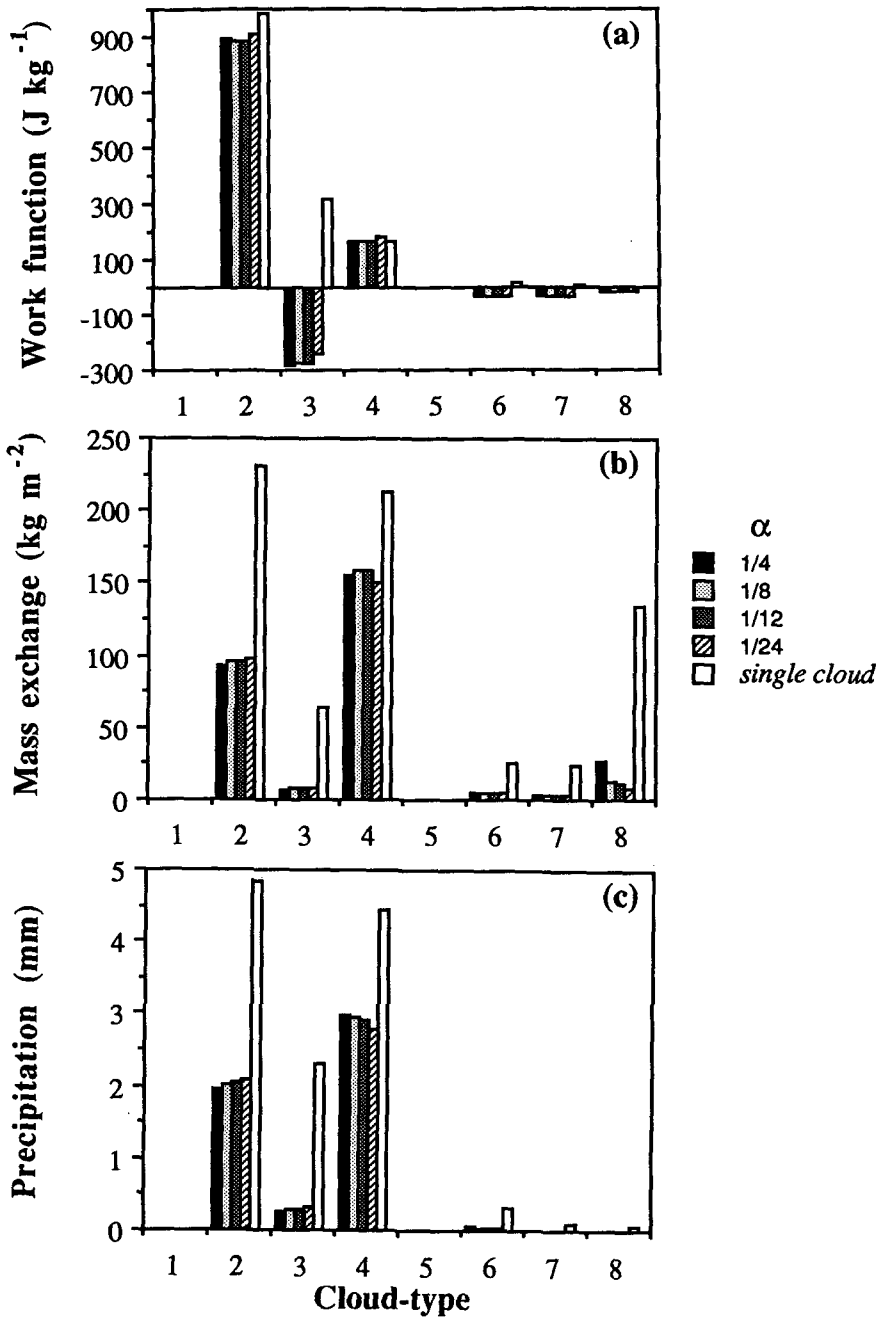

FIG. 6. Results of multicloud experiment as a function of cloud type for four values of α. (a) The final cloud work function (J kg^{-1}), (b) the total mass exchange at the cloud base (kg m^{-2}), and (c) the total precipitation (mm). For comparison, the single-cloud case for cloud type 2 with $\alpha = 1/4$ is also included.

adjusts the profile gradually, recomputing the kernel as it goes. This allows it to account for nonlinear effects. It also results in *larger* mass fluxes for a given forcing, since the tendency is for the diagonal kernel elements to decrease during the adjustment. For the case being discussed, the RAS kernel decreased by 25% during the course of iteration.

Finally, some of the differences are attributable to the different vertical discretizations used for the two schemes. These are fairly large for the shallow clouds, whose vertical extent is close to the grid size. (It is probably for this reason that cloud type 8 appears with RAS in this example.) For deep clouds, like the ones considered here, discretization differences are smaller than the effects already discussed.

As shown in the previous subsection, when multiple cloud types were allowed, RAS produced solutions with nonzero mass fluxes for all possible cloud types (e.g.,

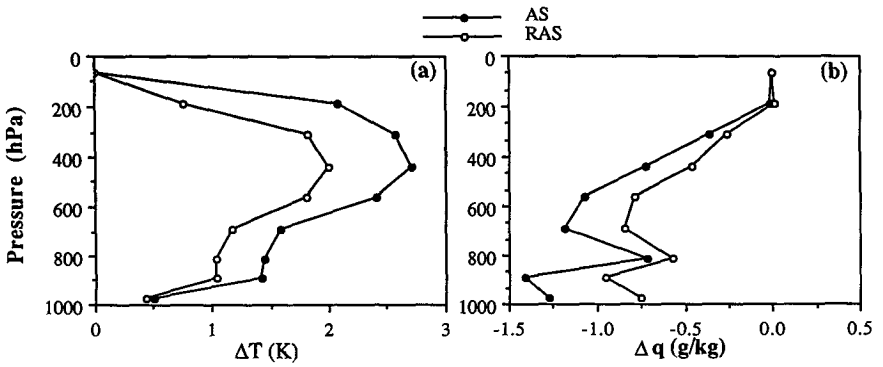

FIG. 7. Vertical profiles of cumulus induced (a) temperature change ΔT (K) and (b) moisture change Δq (g kg^{-1}) for the standard implementation of Arakawa-Schubert and for the RAS single-cloud case (cloud type 2, $\alpha = 1/4$).

Fig. 6b), while the standard implementation overadjusted all but the deepest. It seems reasonable that cloud types 3, 6, and 7 should be eliminated by the standard implementation, since they were also strongly overadjusted and produced very small mass fluxes in the multicloud RAS results. The overadjustment of the cloud type 4, however, is surprising. This cloud was the only one RAS did *not* overadjust, and it made the largest contribution to both the precipitation and the mass flux (see Fig. 6). On closer examination, one finds that cloud type 4 in this case is strongly nonlinear. For the standard implementation, the diagonal kernel element is very large, and therefore the cloud is easily stabilized by other clouds. In RAS, the kernel is also large initially but falls by 70% during the iteration. We suspect that when the standard implementation is called infrequently, such nonlinear situations are common. When they occur, important cloud types may be ignored, while others are spuriously overadjusted. This can lead to clouds being "turned on and off" erratically—a behavior observed when using the standard implementation.

To give some idea of computational efficiency, a vectorized version of RAS is compared with the version (also well vectorized) of the standard implementation used in the GLA model (Sud et al. 1991). Both versions are run in a nine-layer, 4° latitude × 5° longitude version of ARIES GCM at GLA. When all cloud types are invoked sequentially from bottom to top every time step (7.5 min), RAS took ~5 s per simulated day on a single CRAY-YMP processor. The standard implementation took ~80 s per simulated day when invoked as frequently. Of course, since the standard implementation produces a more complete adjustment with each call, it need not be called as frequently. In the GLA model, it is called every half hour, taking approximately 20 s per simulated day. For this case, RAS is approximately four times faster than the standard implementation, with roughly half of the speedup resulting from the linearization of the entrainment relation and the other half from simplification of the solution method. One can expect ever greater economy from RAS when more vertical resolution is used, and relatively fewer clouds are used each time step.

4. Semiprognostic evaluation

In the semiprognostic approach, observations at a given time are used to estimate the large-scale forcing of the cumulus convection, and the cumulus parameterization is used to predict the cumulus precipitation and the warming and drying of the atmosphere. Lord (1978, 1982) used this approach to evaluate the standard AS implementation, and Ramanathan (1980) used it to show predicted precipitation for a monsoon depression formed over the Bay of Bengal. Krishnamurti et al. (1980) used a similar approach to compare the prediction of precipitation rates during Phase III of the GATE using several different cumulus parameterization schemes. Recently, Kao and Ogura (1987) have also used the semiprognostic approach to evaluate an alternate implementation of the AS parameterization. In this section, the semiprognostic approach developed by Lord (1982) is followed. The data and the procedure used are outlined in the next subsection. The results are presented in subsequent subsections.

a. Data and procedure

The large-scale forcing is obtained from the B- and A/B-scale network data for GATE Phase III, as analyzed by Thompson et al. (1979). In this dataset, the values of temperature, specific humidity, their horizontal and vertical derivatives, and all velocity components are given every 3 h at the center of the B-scale array. Data are available at the surface and at 25-hPa intervals from 1000 to 100 hPa. The dataset also contains estimates of the apparent heat source Q_1 and apparent moisture sink Q_2 as defined by Yanai et al. (1973):

$$Q_1 \equiv \frac{\partial s}{\partial t} + \mathbf{V} \cdot \nabla s + \omega \frac{\partial s}{\partial p} \tag{39}$$

and

$$Q_2 \equiv -L\left(\frac{\partial q}{\partial t} + \mathbf{V}\cdot\nabla q + \omega\frac{\partial q}{\partial p}\right), \qquad (40)$$

where $\mathbf{V}$ is the horizontal wind vector, and ω is the vertical p velocity. All other symbols were defined earlier. In addition to the quantities available from the Thompson et al. (1979) dataset, an estimate of the radiative heating is also needed. For this, the daily mean values of the net solar and the infrared cooling rates Q_R tabulated by Cox and Griffith (1978) are used. These data are available as daily mean radiative flux divergences for layers of thickness ~100 hPa. The large-scale forcing of the cloud work function in this semiprognostic study is calculated as discussed in section 2d. At each observation time, the cloud work function is computed based on the observed sounding. Using Q_1, Q_2, Q_R, and a time step Δt of 7.5 min, the sounding is updated and the cloud work function is recomputed. The forcing is then obtained from (38).

b. Results with sequentially invoked cloud types

As discussed earlier, the choices left in RAS are to specify a way to invoke the different cloud types and to specify the iteration parameter (or relaxation time scale) for each cloud type. In this subsection, results are presented for the case where cloud types are invoked sequentially, from bottom to top, as in the previous section and use the same nine-layer model. The calculations are performed for the observed soundings at 3-h intervals from 0000 UTC 1 September to 0000 UTC 18 September. Solutions are presented after complete adjustment (300 iterations using $\alpha = 1/16$) of each of the observed soundings. This is done in order to facilitate direct comparison with a similar study by Lord (1982) using standard implementation of AS. When RAS is used in a GCM, we do not seek complete adjustment every time step; rather, we invoke few cloud types per time step and expect complete adjustment over a period of few hours. Some results in this mode will be presented in section 5.

Figure 8 shows the predicted precipitation rate (solid line) as a function of time. For comparison, an estimate of the precipitation rate obtained from the observed moisture budget by integrating the Q_2 data available in the GATE dataset:

$$P_{Q_2} = \int_{100}^{p_s} \frac{Q_2}{L}\,dp + E, \qquad (41)$$

where P_{Q_2} is the estimate of the precipitation rate, and E is the evaporation rate estimated using bulk aerodynamic formulas (Thompson et al. 1979), has also been plotted (dashed line). It is clear from this figure that the parameterization is quite successful in predicting the estimated rainfall, particularly during disturbed conditions. Comparison of Fig. 8 with Figs. 6 or 12 of Lord (1982) reveals that RAS's prediction of precipitation is comparable to that of the standard implementation.

It should be remarked at this stage that it is somewhat misleading to compare the predicted and the observed precipitation. In fact, even the simple assumption that the precipitation equals the vertically integrated moisture flux convergence [this is equivalent to ignoring the contribution of local rate of change of moisture in (41)] gives quite a good estimate of the precipitation. It should also be recognized that it is not good enough to predict the total precipitation; it is more important to correctly predict the vertical profiles of the cumulus heating and drying. RAS, as well as Arakawa–Schubert, accomplish this through the cloud model and the closure assumption of quasi equilibrium of the work function.

Figures 9a,b show vertical profiles of the time-averaged (from 0000 UTC 1 September to 0000 UTC

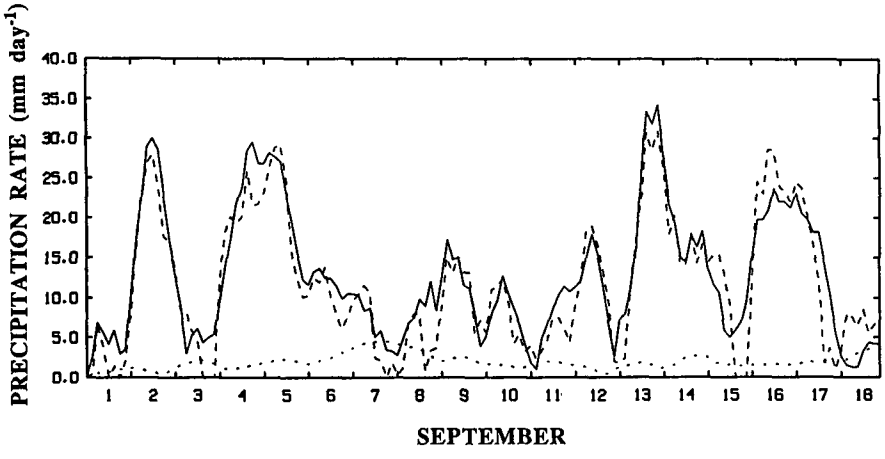

FIG. 8. Time evolution of the precipitation rate (mm day^{-1}) predicted semiprognostically by RAS (the solid curve) using a nine-layer model with sequentially invoked cloud types (see text for details) and $\alpha = 1/16$. An estimate of the precipitation from the GATE observations (the dashed curve) is also shown, along with an estimate of evaporation (the dotted curve).

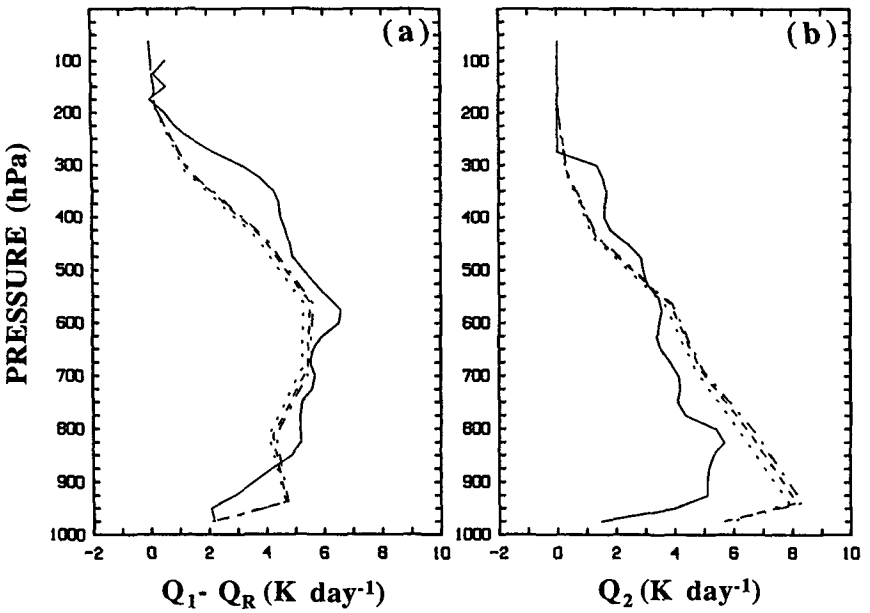

FIG. 9. Vertical profiles of time-averaged (a) $Q_1 - Q_R$ (K day^{-1}) and (b) Q_2 (K day^{-1}) obtained in the semiprognostic study with sequentially invoked cloud types. The solid curve is an observed estimate. The dotted, dashed, and the dash-dotted curves are for $\alpha = 1/4$, $\alpha = 1/8$, and $\alpha = 1/16$, respectively.

18 September) cumulus warming and drying produced by RAS (dotted lines). The corresponding observed estimates of warming and drying from the GATE data are also shown (solid lines). The predicted warming seems to underestimate the observed, and the predicted drying overestimates the observed at lower levels. This problem also exists in the standard implementation of AS (see Lord 1982; Fig. 12). Recently, Cheng and Arakawa (1990) have shown that this excessive low-level drying is reduced when cumulus-induced downdrafts are taken into account. Inclusion of reevaporation of falling rain (Sud and Molod 1988) can also reduce the problem. Neither of these effects is included in our scheme at this time, but they can be easily added. Their direct inclusion in the mass-flux calculation would involve modification of the kernel. However, in RAS, these effects can be included externally, without modifying the kernel, by letting them affect cloud interaction iteratively. In other words, after invoking a cloud type, one can include the effects of downdrafts and/or reevaporation of falling rain before invoking another cloud type.

Figures 10a and 10b show the distribution of predicted (cumulus induced) warming, $Q_1 - Q_R$, and drying, Q_2, as a function of time and pressure. For comparison, Figs. 11a and 11b present an estimate of observed $Q_1 - Q_R$ and Q_2 [obtained from the GATE dataset of Thompson et al. (1979) and from the daily mean values presented in Cox and Griffith (1978)]. We see that the predicted cumulus warming and drying are in good agreement with the observed estimates, particularly during disturbed situations. However, the vertical extent of the heating and drying estimated by the parameterization is somewhat lower than observed. This may be partially due to the fact that the model is unable to resolve the deepest cloud on this coarse grid. Similar results were also found for other values of the parameter α_i and are therefore not presented here.

Next, to assess the impact of vertical resolution (or increased number of cloud types), the above calculations were repeated with a 20-layer model using a uniform layer thickness of $\Delta\sigma = 0.05$. Again, all cloud types were invoked sequentially from bottom to top. The results are similar to those presented above; therefore, only the time-averaged heating and drying in Figs. 12a,b are presented. As in Fig. 9, the predicted warming agrees quite well with the observed estimate, while the low-level drying is overestimated. However, the time-mean warming is better in the 20-layer case than in the 9-layer case, especially at lower levels, while the drying at lower levels is slightly worse. This must be due to the fact that the 20-layer case has more cloud types with the possibility of having more mass flux in deeper cloud types. This would result in increased mass flux at all levels (except possibly in the near lowest few levels, where the mass flux due to shallow cloud types may be reduced due to the presence of more deep cloud), resulting in increased heating and drying. Better accuracy in estimating the vertical derivatives may also play some role. The above experiments were repeated for other values α_i with similar results.

c. *Results with randomly invoked cloud types*

In this subsection, results from a semiprognostic study in which randomly chosen cloud types were in-

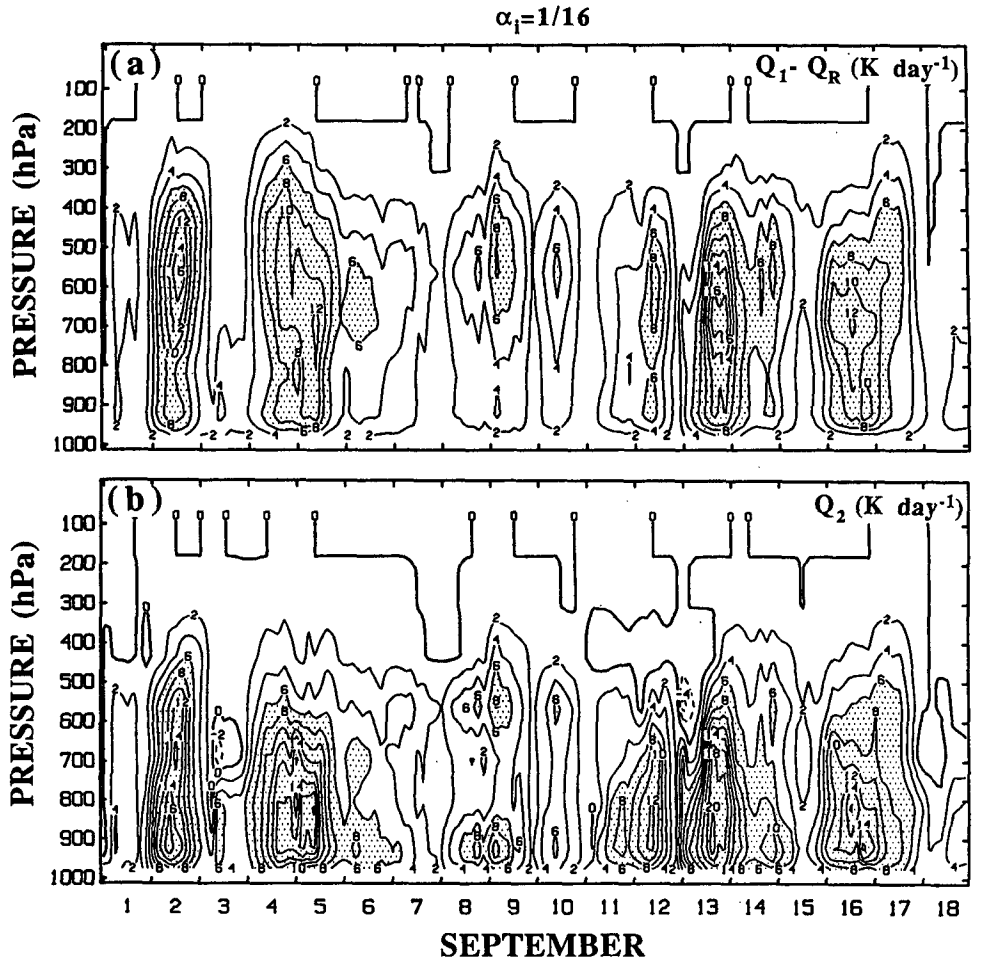

FIG. 10. Pressure–time cross sections of (a) $Q_1 - Q_R$ (K day^{-1}) and (b) Q_2 (K day^{-1}) for the case in Figs. 8 and 9.

voked are discussed. The nine-layer case is considered. In this case, eight cloud types (reaching layers one through eight) are possible. The cloud types were randomly selected from this pool.

Figures 13a and 13b show the precipitation as a function of time for α_i = 1/4 after invoking 50 and 1500 randomly selected cloud types, respectively. Comparing either with Fig. 8, results are found to be very similar to those with sequentially invoked cloud types; comparing the two reveals that the soundings have been almost fully adjusted by the time 50 cloud types are invoked, or when each cloud type has been invoked approximately six times on average. In the nine-level GCM tests, for which timings were quoted, all clouds were invoked sequentially every 7.5 min. This results in 192 clouds every 3 h. Since 50 randomly invoked clouds are sufficient to equilibrate, a further economy of roughly a factor of 4 could be obtained by demanding approximate equilibrium only on time scales longer than 3 h.

The time–pressure cross sections of the cumulus warming and drying, as well as the vertical profile of their time means, are very similar to those presented for the sequentially invoked case. The above calculations were also repeated for many other values of α_i and for the 20-layer case with similar results.

5. Prognostic evaluation

In this section, the performance of RAS in a fully prognostic mode is discussed. This approach is similar to that used by Betts and Miller (1986) and Tiedtke (1989) to evaluate their parameterizations. Both Betts–Miller and Tiedtke performed the prognostic test (involving integrations over a few days covering a full wave period) using the composite wave data for the GATE Phase III. The same data used in section 4 will be used, namely, the A/B-scale array data for the Phase III of GATE.

The same nine-layer version of the model discussed in the previous sections will also be used. Starting from an initial sounding from the GATE data, the thermodynamic and moisture equations are numerically integrated to forecast future temperature and moisture profiles for the whole GATE Phase III period. For this

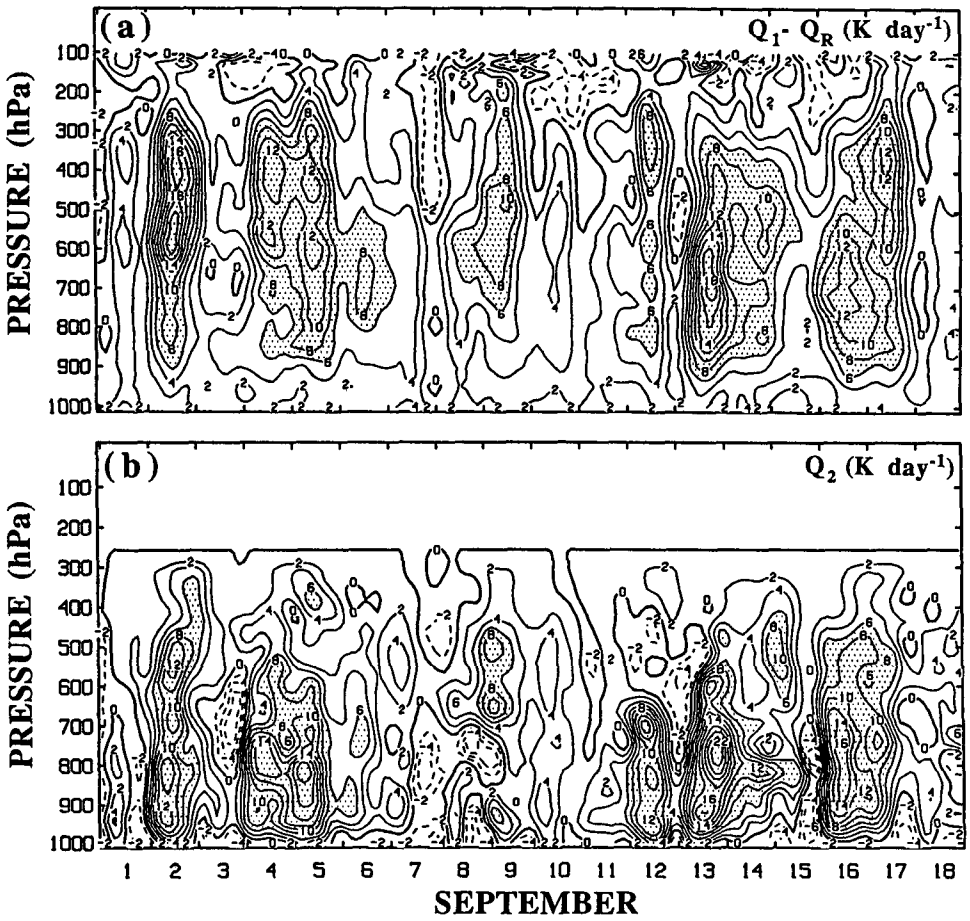

FIG. 11. As in Fig. 10, but for the observed estimate for GATE [from Thompson et al. (1979) and Cox and Griffith (1978)].

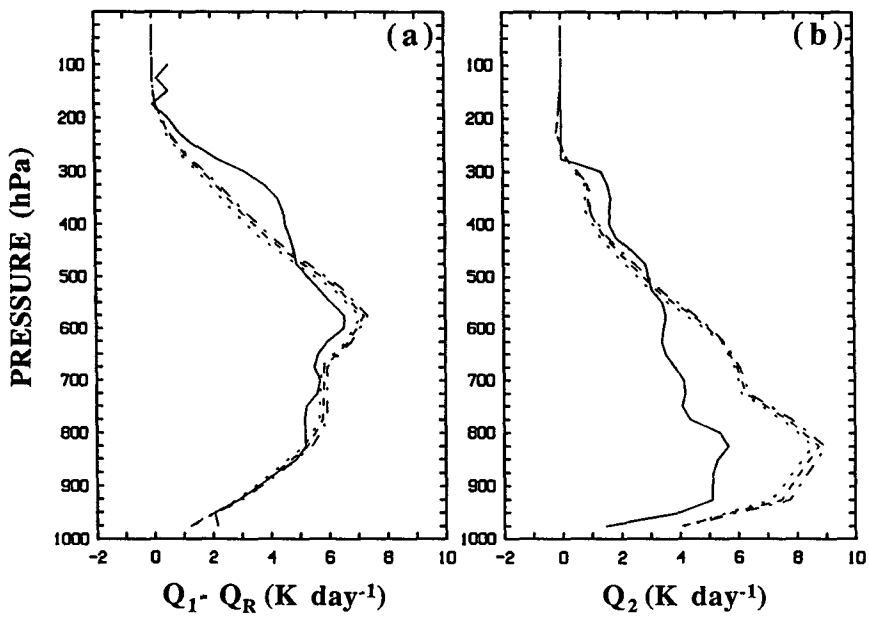

FIG. 12. Same as in Fig. 9, but for a 20-layer model.

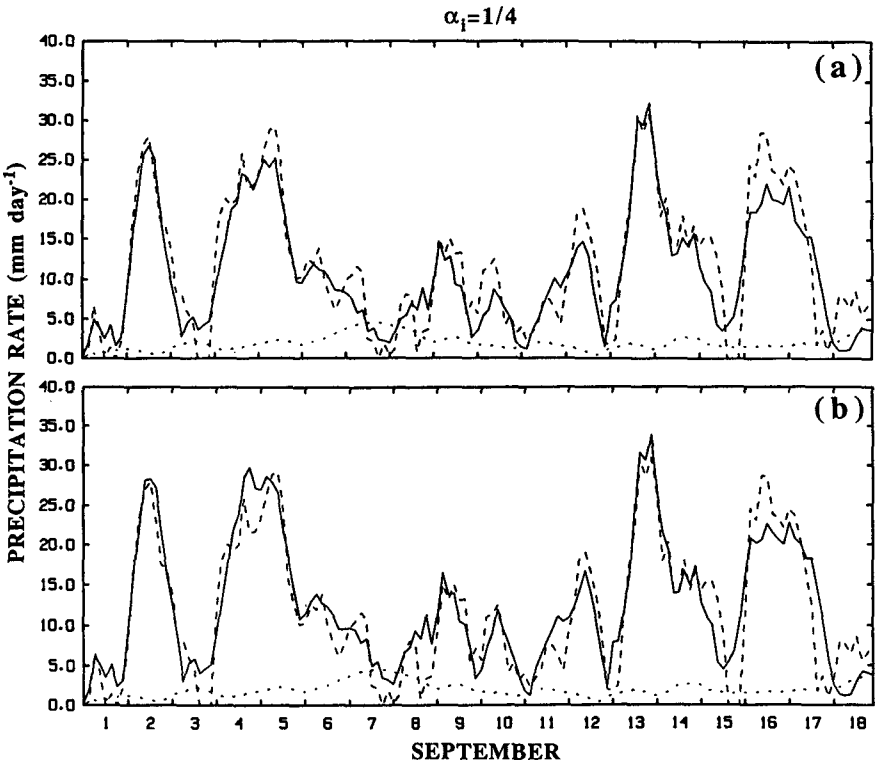

FIG. 13. Same as in Fig. 8, but after randomly invoking (a) 50 cloud types and (b) 1500 cloud types for α = 1/4.

purpose, the advective time changes of temperature and moisture were again obtained from the observed estimates given by Thompson et al. (1979) and the contributions from the sensible and latent heat fluxes from the lower boundary were evaluated using bulk formulas. No turbulent flux across the top of the lowest model layer was assumed. Radiative effects were included from the daily mean data from Cox and Griffith (1978). It was found that the Q_1 and Q_2 from Thompson et al. (1979) were not consistent with the Q_R values from Cox and Griffith (1978) when vertically integrated and time averaged. Therefore, the vertical profiles of the radiative heating were modified by multiplying them by a constant factor so that the time mean of the vertically integrated $Q_1 - Q_R$ balanced the time-mean vertically integrated Q_2.

The integration was started at 2100 UTC 31 August and was carried out until 0000 UTC 19 September. The cumulus effects were calculated prognostically using RAS in the same way it would be used in the GCM. The large-scale forcing was calculated as the ratio of the excess of work function above a critical value to the time step, as in section 2d. The critical work function was taken from LCA. In this experiment, all eight cloud types were invoked sequentially from bottom to top for each time step. A time step of 450 s was used. To approximate the complete equilibrium results, a larger value of the relaxation parameter (α_i = 1/2) than has been considered thus far was used, corresponding to a typical single-cloud adjustment time scale ($\tau_i = \Delta t/\alpha_i$) of 15 min. A parameterization of precipitation due to grid-scale supersaturation and a scheme for dry convective adjustment were also included. In the large-scale precipitation scheme, it was assumed that when a layer is supersaturated, condensation occurs and the condensate falls to the layer below, where it is reevaporated. Precipitation is realized at the ground only when the lowest layer is supersaturated.

Figure 14 shows the time evolution of predicted convective precipitation (large-scale precipitation is small, never exceeding 1 mm day^{-1}). For comparison, the observed estimate of precipitation (dashed line) and evaporation (dotted line) from Fig. 8 are also replotted. The predicted rainfall agrees quite well with the observed estimate for most of the events occurring during this period, except near days 8–10. It is not very clear why the model performed poorly during this period. The inaccuracies resulting from using a daily mean and vertically coarse radiation data or the inaccurate estimates of surface fluxes may be responsible for the differences.

The predicted total $Q_1 - Q_R$ and Q_2 as a function of time and pressure are shown in Figs. 15a,b. Comparing these figures with Figs. 10a,b shows that RAS has been able to capture all wave disturbances reasonably well, except around day 9, when strong cooling

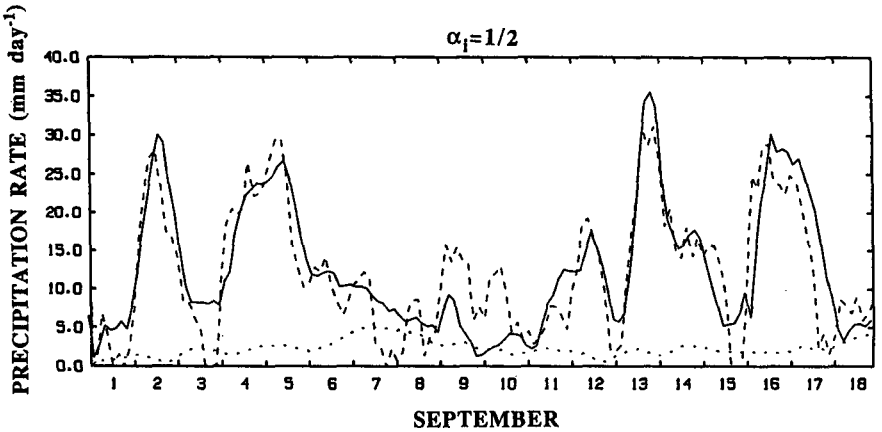

FIG. 14. Predicted cumulus precipitation rate (mm day^{-1}) for the prognostic case with $\alpha = 1/2$.

and moistening occurred in the lower troposphere due to large-scale precipitation. The predicted temperature and specific-humidity profiles as a function of time are shown in Figs. 16a and 16b. For comparison, Figs. 17a,b also present corresponding observed fields for GATE. Comparing these figures, note that the predicted fields are somewhat warmer and too dry, particularly at lower levels. Inclusion of downdrafts or evaporation of falling rain might help to reduce this difference.

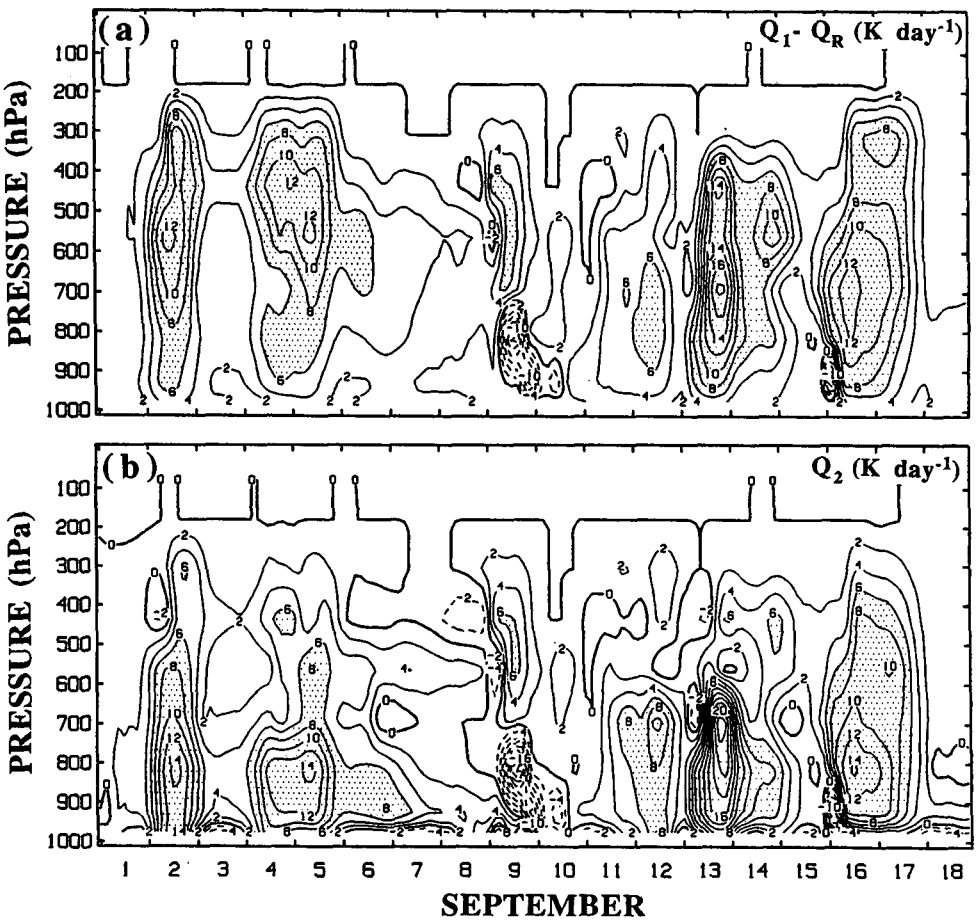

FIG. 15. Predicted total (a) $Q_1 - Q_R$ (K day^{-1}) and (b) Q_2 (K day^{-1}) for the prognostic case.

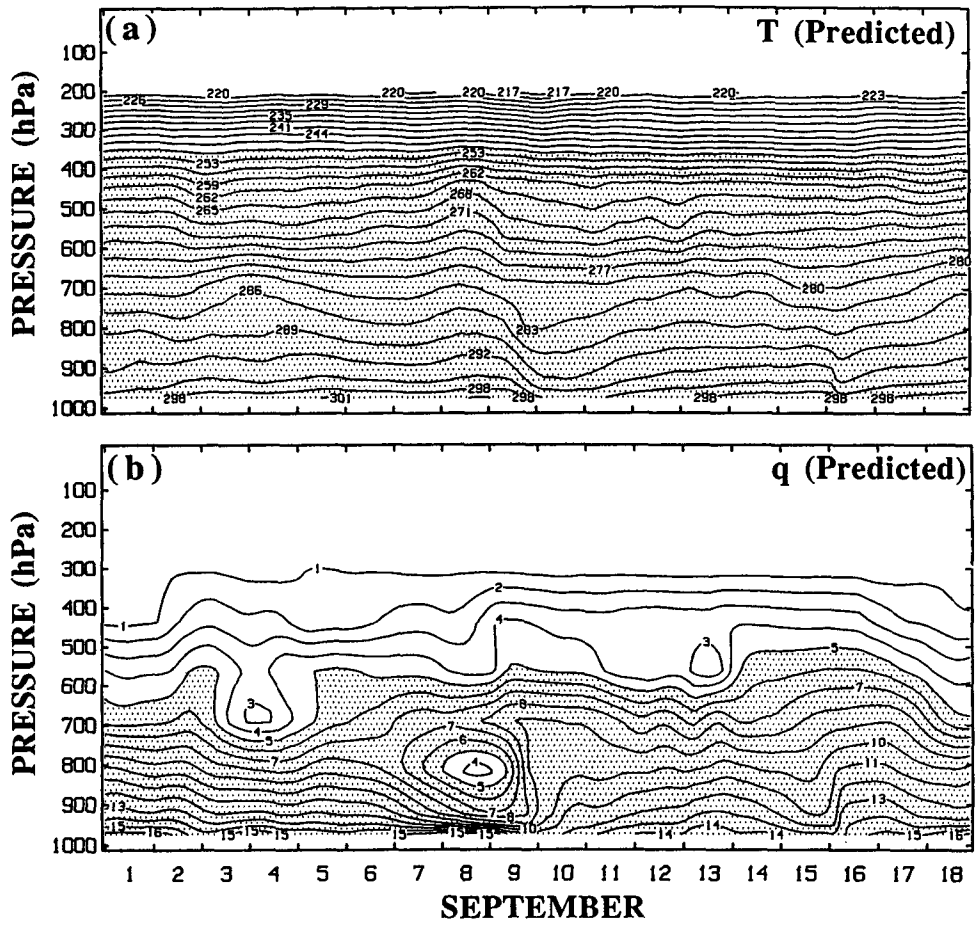

FIG. 16. Time–pressure cross section of predicted (a) temperature (K) and (b) specific humidity (g kg^{-1}).

We can see from Fig. 17b that between 8 and 9 September there was a large drying event near the 800-hPa level. This must have been due to moisture divergence from the column during this period. The prognostic study somewhat overemphasized this event and produced strong drying near the same level, partly because of the excessive drying at lower levels. Around 9 September, the moisture in the middle and lower troposphere increased; this led to supersaturation in the upper layers and large-scale condensation. Observations do suggest some evidence of heating and moistening at upper levels and drying at lower levels during this period (Figs. 11a,b). A similar situation seems to have occurred around 15 and 16 September.

It should again be emphasized that the prognostic test may be somewhat misleading. Since the large-scale forcing is prescribed, the time-mean heating and drying are effectively prescribed. As mentioned before, even the simplest parameterization in which vertically integrated moisture flux convergence is treated as precipitation can perform reasonably well if a proper choice of vertical profile is made.

6. Summary and conclusions

In this paper, we presented a simple implementation of the fundamental ideas in the convective cloud parameterization of Arakawa and Schubert (1974). RAS makes two major simplifications to the standard AS implementation by modifying the entrainment relation and by relaxing the state toward equilibrium, rather than requiring complete quasi equilibrium. The details of the implementation are given in section 2 and the Appendix.

We studied the sensitivity of each cloud type to the value of the relaxation parameter using a nine-layer version of the model and a sounding from the ECMWF analysis. We found that the solutions for all relaxation parameters converge to the same solution and compared it with that obtained from the standard implementation. This comparison suggested that the solution produced by RAS is not only unique, but also may be physically more realistic because it does not depend on minimization of some arbitrary functional, as in the simplex solution of the standard implementation.

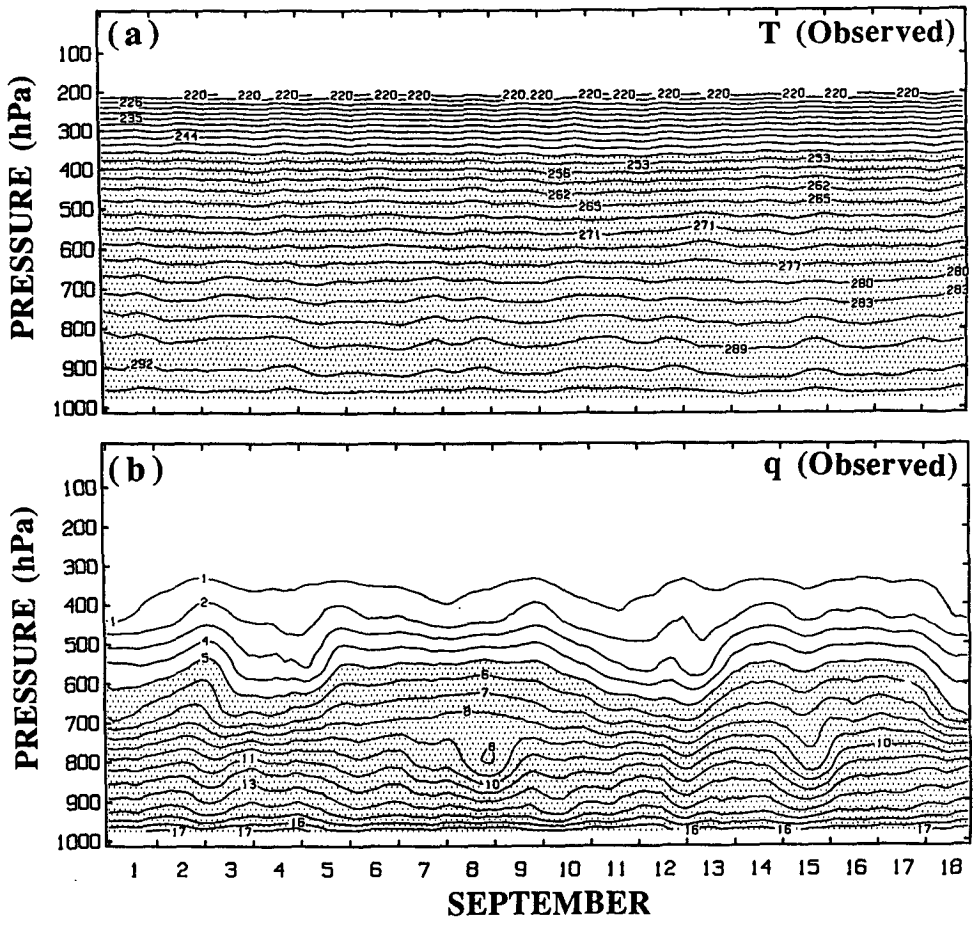

FIG. 17. Same as in Fig. 16, but from GATE Phase III observations.

We performed a semiprognostic evaluation of RAS using GATE Phase III data and following the approach used by Lord (1978, 1982). We found that RAS produces good estimates of the precipitation, as well as of the vertical profiles of heating and drying. The scheme does overestimate the drying in the lower troposphere, as does the standard implementation of AS. We also showed that with a sufficiently large value of the relaxation parameter, invoking ~50 random cloud types is sufficient to produce precipitation, as well as heating and drying fields similar to those observed.

We also performed a prognostic evaluation of RAS using the GATE data. The precipitation and heating and drying due to convection were predicted, while the advection, surface fluxes, and radiative processes were prescribed from observation. This test produced reasonably good estimates of precipitation rate and cumulus-induced heating and drying.

RAS can be easily implemented in any large-scale numerical prediction model by invoking several cloud types for each time step. Because we partially adjust each sounding for one cloud type at a time and let cloud interactions take place iteratively, even a crude representation of the diagonal element of the kernel matrix can converge to the right solution. Thus, one can use, for example, the cloud model in this paper and include the reevaporation of falling precipitation outside of RAS after invoking each cloud type and letting its effect be felt during the course of iteration. Of course, any change to the cloud model can also be easily included in the scheme.

One problem that might arise in a prognostic model, particularly with rather coarse vertical resolution, is that during the integration, a deep cloud that was previously inactive might become active, producing discontinuities or spikes in the precipitation and the heating rates. This can be avoided by allowing the ith cloud type to become active as soon as the cloud top corresponding to the deepest possible cloud (the nonentraining cloud) lies anywhere between the levels i and $i + 1$, thus making the transition more or less continuous.

We have used RAS with the above modification in the ARIES GCM at Goddard Laboratory for Atmospheres. For a nine-layer GCM with a resolution of 4° latitude × 5° longitude resolution, RAS needs ~5 s

per simulated day on a single CRAY-YMP processor when eight cloud types are invoked at each dynamics time step (7.5 min). Further reduction in computer time can be expected by pursuing other calling strategies.

Acknowledgments. We thank Professor Akio Arakawa and Dr. Stephen J. Lord for many valuable discussions and two anonymous reviewers for their thoughtful reviews. We also thank Ms. Laura Rumburg for helping with some of the figures. This work was supported by the Modeling, Data, and Information System Program Office of NASA headquarters.

APPENDIX

The Discrete Version of the Parameterization

a. The cloud model

Here the discrete version of the cloud model is described, which is similar to that used in Lord et al. (1982), differing primarily in the entrainment relation and in the details of the discretization. Each cloud type is identified by its detrainment level. Let us say we have a K-layer model, and the variables associated with the layers will be identified by integer subscripts and those associated with the interface levels by half-integer subscripts (see Fig. A1).

All clouds are assumed to have the same base. In a GCM, this is usually taken as the top of the lowest layer, although a more sophisticated choice (such as some average of the lowest few layers in models that attempt to resolve the boundary layer explicitly) could be easily implemented. We will refer to that cloud type with its top (detrainment level) in layer i, as the ith cloud type.

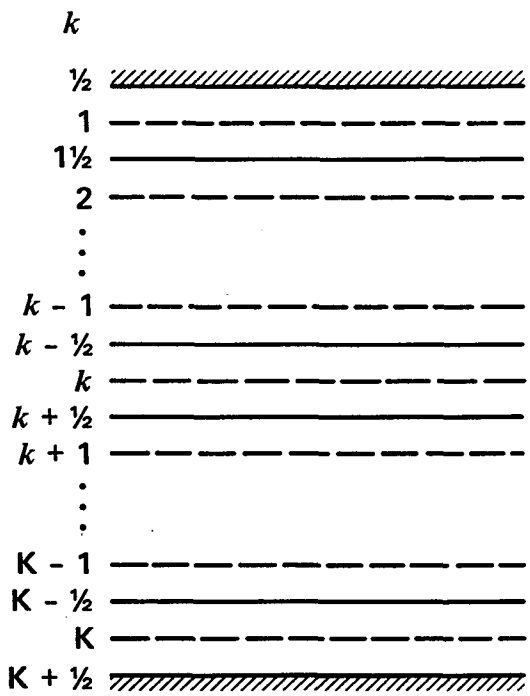

FIG. A1. Schematic of a vertically discrete model.

Assuming that the normalized mass flux for each cloud type is a linear function of height,

$$\eta_{i,k-1/2} - \eta_{i,k+1/2} = \lambda_i(z_{k-1/2} - z_{k+1/2}), \quad k = i+1, i+2, \cdots K-1, \quad \text{(A1)}$$

where $\eta_{i,k+1/2}$ is the cloud mass flux of the ith cloud type at level $k + 1/2$ normalized by its value at the cloud base, λ_i is its entrainment rate, and $z_{k+1/2}$ is the height of level $k + 1/2$. Equation (A1) applies from the layer immediately below the detrainment layer to the layer immediately above the cloud base, which, for the purpose of this discussion, is assumed to be at $K - 1/2$. We arbitrarily assume that detrainment occurs at the middle of the detrainment layer and therefore that there is an additional half-layer at the top over which the cloud entrains:

$$\eta_{i,i} - \eta_{i,i+1/2} = \lambda_i(z_i - z_{i+1/2}). \quad \text{(A2)}$$

The vertical coordinate is specified by the pressures at the half-integer levels ($p_{k+1/2}$, $k = 1, 2, \cdots K$). We will thus need a discrete hydrostatic relation for the thickness on the rhs of (A1) and (A2). The form of the hydrostatic equation proposed by Arakawa and Suarez (1983) is used, which is also the form used in ARIES GCM:

$$z_{k-1/2} - z_{k+1/2} = \frac{c_p}{g}\theta_k(P_{k+1/2} - P_{k-1/2}), \quad k = 1, 2, \cdots K \quad \text{(A3)}$$

over the full layers and

$$z_k - z_{k+1/2} = \frac{c_p}{g}\theta_k(P_{k+1/2} - P_k), \quad k = 1, 2, \cdots K \quad \text{(A4)}$$

over the lower half of each layer. Here θ_k is the potential temperature of layer k,

$$P_{k+1/2} = (p_{k+1/2}/p_0)^\kappa, \quad \text{(A5)}$$

and

$$P_k = \frac{1}{1+\kappa}\left(\frac{P_{k+1/2}p_{k+1/2} - P_{k-1/2}p_{k-1/2}}{p_{k+1/2} - p_{k-1/2}}\right), \quad \text{(A6)}$$

which is the form suggested by Phillips (1974) and used in Arakawa and Suarez (1983). Here $\kappa \equiv R/c_p$.

Using (A3) and (A4) in (A1) and (A2),

$$\eta_{i,k-1/2} - \eta_{i,k+1/2} = \beta_k\theta_k\lambda_i, \quad k = i+1, i+2, \cdots K-1, \quad \text{(A7)}$$

where

$$\beta_k = \frac{c_p}{g}(P_{k+1/2} - P_{k-1/2}). \quad \text{(A8)}$$

For the last half-layer up to the detrainment level,

$$\eta_{i,i} = \eta_{i,i+1/2} + \beta_i\theta_i\lambda_i, \quad \text{(A9)}$$

where

$$\beta_i = \frac{c_p}{g}(P_{i+1/2} - P_i). \quad \text{(A10)}$$

Summing (A7) and combining with (A9), we obtain the following form for the normalized mass flux at the detrainment level:

$$\eta_{i,i} = 1 + \lambda_i \sum_{K-1}^{i} \beta_k\theta_k, \quad \text{(A11)}$$

where $\eta_{i,K-1/2} = 1$ is used.

Similarly, the discrete form of the moist static energy budget of each cloud type can be obtained. Let $h_k = s_k + Lq_k$ be the moist static energy of layer k, where $s_k = c_pT_k + gz_k$ is the dry static energy, $T_k = P_k\theta_k$ is the temperature, and q_k is the specific humidity of layer k. Here θ_k and q_k are prognostic variables of the GCM and thus are known. Then h_k and s_k are also known. Thus,

$$\eta_{i,k-1/2}h^c_{i,k-1/2} - \eta_{i,k+1/2}h^c_{i,k+1/2} = (\eta_{i,k-1/2} - \eta_{i,k+1/2})h_k, \quad k = i+1, i+2, \cdots K-1, \quad \text{(A12)}$$

where $h^c_{i,k+1/2}$ is the cloud moist static energy of the ith cloud type at level $k + 1/2$. The rhs of (A12) represents the effect of entraining environmental air over layer k. For the half-layer at the cloud top we write

$$\eta_{i,i}h^c_{i,i} - \eta_{i,i+1/2}h^c_{i,i+1/2} = (\eta_{i,i} - \eta_{i,i+1/2})h_i. \quad \text{(A13)}$$

Summing (A12) and combining with (A13), we obtain the following expression for the cloud-top moist static energy:

$$\eta_{i,i}h^c_{i,i} = h_K + \sum_{K-1}^{i+1} (\eta_{i,j-1/2} - \eta_{i,j+1/2})h_j + (\eta_{i,i} - \eta_{i,i+1/2})h_i. \quad \text{(A14)}$$

Ignoring precipitation, an equation similar to (A12) can be written for cloud total water:

$$\eta_{i,k-1/2}(q^c_{i,k-1/2} + l_{i,k-1/2}) - \eta_{i,k+1/2}(q^c_{i,k+1/2} + l_{i,k+1/2}) = (\eta_{i,k-1/2} - \eta_{i,k+1/2})q_k, \quad k = i+1, i+2, \cdots K-1, \quad \text{(A15)}$$

where $q^c_{i,k+1/2}$ and $l_{i,k+1/2}$ are the specific humidity and the liquid water mixing ratio of the ith cloud type at level $k + 1/2$. The rhs of (A15) assumes no liquid water in the environment. From (A15), assuming $q^c_{i,i} = q^*_i$, where q^*_i is the saturation specific humidity of layer i, we obtain:

$$l_{i,i} = \frac{1}{\eta_{i,i}}\left[q_K + \sum_{K-1}^{i+1} (\eta_{i,j-1/2} - \eta_{i,j+1/2})q_j + (\eta_{i,i} - \eta_{i,i+1/2})q_i\right] - q^*_i \quad \text{(A16)}$$

Here $l_{i,i}$ is the liquid water mixing ratio of the detraining air for the ith cloud type. Since θ and q are known and the saturation specific humidity can be calculated, $l_{i,i}$ can be calculated if λ_i is known.

Neglecting virtual effects and liquid water loading, the level of nonbuoyancy for each cloud type is that at which

$$h^c_{i,i} = h^*_i, \quad \text{(A17)}$$

where $h^c_{i,i}$ depends on the entrainment parameter λ_i, and $h^*_i = s_i + Lq^*_i$ is the saturation moist static energy of layer i. Substituting for $h^c_{i,i}$ from (A14) and using the entrainment relations (A1) and (A2), an expression for λ_i is obtained as

$$\lambda_i = \frac{h_K - h^*_i}{\sum_{K-1}^{i} \beta_j\theta_j(h^*_i - h_j)}. \quad \text{(A18)}$$

In the standard AS implementation, (A17) is a polynomial in λ_i whose degree depends on the height of the detrainment level.

b. *The cloud work function*

The discrete form of the cloud work function is obtained by discretizing (16) of section 2. Since at this point the normalized mass flux and the cloud moist static energy at the half-integer levels from (A1), (A2), and (A12) and the saturation moist static energy at the GCM layers are known, we adopt the following quadrature for (16):

$$A_i = \sum_{K-1}^{i+1} [\epsilon_j\eta_{i,j+1/2}(h^c_{i,j+1/2} - h^*_j) + \mu_j\eta_{i,j-1/2}(h^c_{i,j-1/2} - h^*_j)] + \epsilon_i\eta_{i,i+1/2}(h^c_{i,i+1/2} - h^*_i), \quad \text{(A19)}$$

where A_i is the cloud work function for the ith cloud type and the definitions:

$$\epsilon_j \equiv \frac{P_{j+1/2} - P_j}{P_j(1 + \gamma_j)}, \quad j = 1, 2, \cdots K-1 \quad \text{(A20)}$$

and

$$\mu_j \equiv \frac{P_j - P_{j-1/2}}{P_j(1 + \gamma_j)}, \quad j = 1, 2, \cdots K-1 \quad \text{(A21)}$$

are used. Using (A12) to eliminate the cloud moist static energy h^c (A19) can finally be written in terms of environmental quantities only:

$$A_i = \epsilon_{K-1}h_K - \epsilon_i\eta_{i,i+1/2}h_i^* + \sum_{K-1}^{i+1}(\epsilon_{k-1} + \mu_k) \times [h_K + \sum_{K-1}^{k}(\eta_{i,j-1/2} - \eta_{i,j+1/2})h_j] - \sum_{K-1}^{i+1}[\epsilon_k\eta_{i,k+1/2} + \mu_k\eta_{i,k-1/2}]h_k^*. \quad \text{(A22)}$$

c. Cumulus effects on the large-scale budgets

The cumulus effects on the budgets of dry and moist static energies for the environment are discretized as

$$\left(\frac{\partial s_k}{\partial t}\right)_c = \frac{g}{\Delta p_k}[M_{k-1/2}(s_{k-1/2} - s_k) + M_{k+1/2}(s_k - s_{k+1/2}) - D_k l_k L(1 - r_k)] \quad \text{(A23)}$$

and

$$\left(\frac{\partial h_k}{\partial t}\right)_c = \frac{g}{\Delta p_k}[M_{k-1/2}(h_{k-1/2} - h_k) + M_{k+1/2}(h_k - h_{k+1/2}) + D_k(h_k^* - h_k)], \quad \text{(A24)}$$

where $(\partial s_k/\partial t)_c$ and $(\partial h_k/\partial t)_c$ are the rate of change of dry and moist static energies of layer k, $M_{k+1/2}$ is the cumulus mass flux at level $k + 1/2$, and D_k is the detrained mass at level k and $\Delta p_k = p_{k+1/2} - p_{k-1/2}$. The last term on the rhs of (A23) represents cooling from the reevaporation of liquid water detrained to the environment. Here l_k is the liquid water mixing ratio, and r_k is a cloud-type–dependent precipitation fraction. The dry static energy at the level $k + 1/2$ is obtained using the discretization given by Arakawa and Suarez (1983). The specific humidity at this level is taken as the average between levels k and $k + 1$. At the top of the bottom layer, we also experimented by setting $q_{K-1/2}$ to q_K and q_{K-1}.

In the standard AS implementation, $M_{k+1/2}$ would be the total mass flux of all cloud types penetrating the level $k + 1/2$:

$$M_{k+1/2} = \sum_{i=1}^{k} M_B(i)\eta_{i,k+1/2}, \quad \text{(A25)}$$

where $M_B(i)$ is the cloud-base mass flux for the ith cloud type. In RAS, however, only one cloud type is considered at a time, and we use the forms

$$M_{k+1/2} = \begin{cases} M_B(i)\eta_{i,k+1/2} & \text{for } i < k, \\ 0 & \text{for } i \geq k, \end{cases} \quad \text{(A26)}$$

and

$$D_k = \begin{cases} M_B(i)\eta_{i,i} & \text{for } i = k, \\ 0 & \text{for } i \neq k. \end{cases} \quad \text{(A27)}$$

Also, $l_k = l_{i,i}$ is taken for $i = k$, and $l_k = 0$ otherwise. Then (A23) and (A24) can be rewritten as

$$\left(\frac{\partial s_k}{\partial t}\right)_c = M_B(i)\Gamma_s(k) \quad \text{(A28)}$$

and

$$\left(\frac{\partial h_k}{\partial t}\right)_c = M_B(i)\Gamma_h(k), \quad \text{(A29)}$$

where

$$\Gamma_s(k) = \begin{cases} \frac{g}{\Delta p_k}[\eta_{i,k-1/2}(s_{k-1/2} - s_k) + \eta_{i,k+1/2} \times (s_k - s_{k+1/2}) - \eta_{i,i}l_{i,i}L(1 - r_i)\delta_i^k], \\ \qquad \text{for } k = i, i+1, \cdots K, \\ 0 \quad \text{for } k = 1, 2, \cdots i - 1, \end{cases} \quad \text{(A30)}$$

and

$$\Gamma_h(k) = \begin{cases} \frac{g}{\Delta p_k}[\eta_{i,k-1/2}(h_{k-1/2} - h_k) + \eta_{i,k+1/2} \times (h_k - h_{k+1/2}) + \eta_{i,i}(h_i^* - h_i)\delta_i^k], \\ \qquad \text{for } k = i, i+1, \cdots K, \\ 0 \quad \text{for } k = 1, 2, \cdots i - 1. \end{cases} \quad \text{(A31)}$$

Here δ_i^k is the Kronecker delta and it is assumed that $\eta_{i,i-1/2} = \eta_{i,K+1/2} = 0$. From (A28) and (A29), the rate of change of potential temperature and specific humidity due to the ith cloud type can be written as:

$$\left(\frac{\partial \theta_k}{\partial t}\right)_c = \frac{M_B(i)}{c_p P_k}\Gamma_s(k), \quad k = 1, 2, \cdots K, \quad \text{(A32)}$$

and

$$\left(\frac{\partial q_k}{\partial t}\right)_c = \frac{1}{L}M_B(i)[\Gamma_h(k) - \Gamma_s(k)], \quad k = 1, 2, \cdots K. \quad \text{(A33)}$$

d. The mass-flux kernel and cloud-base mass flux

In the discrete model, the equation analogous to (34) of section 2 becomes (LCA),

$$\left(\frac{dA_i}{dt}\right)_c = \sum_j K_{i,j}M_B(j), \quad \text{(A34)}$$

where the summation is over all existing cloud types. In the present case of a single cloud type, only the diagonal element $K_{i,i}$ is available, which is simply given by

$$K_{i,i} = \frac{1}{M_B(i)}\left(\frac{dA_i}{dt}\right)_c. \tag{A35}$$

Then, from (A22) by using (A18), (A28), (A29), (A30), (A31), and the approximate relation

$$\frac{\partial h_k^*}{\partial t} = (1 + \gamma_k)\frac{\partial s_k}{\partial t}, \tag{A36}$$

we obtain

$$K_{i,i} = (\epsilon_{K-1} + \vartheta)\Gamma_h(K) - (\epsilon_i\eta_{i,i+1/2} + \vartheta\eta_{i,i})(1 + \gamma_i)\Gamma_s(i)$$
$$+ \sum_{K-1}^{i+1}\{(\epsilon_{k-1} + \mu_k)[\Gamma_h(K) + \sum_{K-1}^{k}(\eta_{i,j-1/2} - \eta_{i,j+1/2})\Gamma_h(j)] + \vartheta(\eta_{i,k-1/2} - \eta_{i,k+1/2})\Gamma_h(k)\}$$
$$+ \vartheta(\eta_{i,i} - \eta_{i,i+1/2})\Gamma_h(i) - \sum_{K-1}^{i+1}(\epsilon_k\eta_{i,k+1/2} + \mu_k\eta_{i,k-1/2})(1 + \gamma_k)\Gamma_s(k), \tag{A37}$$

where

$$\vartheta = -\epsilon_i h_i^*\eta_{i,i+1/2} + \sum_{K-1}^{i+1}(\epsilon_{k-1} + \mu_k)[\sum_{K-1}^{k}(\eta_{i,j-1/2} - \eta_{i,j+1/2})h_j]$$
$$- \sum_{K-1}^{i+1}[\epsilon_k\eta_{i,k+1/2} + \mu_k\eta_{i,k-1/2}]h_k^* + \epsilon_i h_i^* + \sum_{K-1}^{i+1}(\epsilon_k + \mu_k)h_k^*, \tag{A38}$$

and, for simplicity, we have ignored the rate of change of ϵ and μ. The rate of change of λ_i is included through the terms involving ϑ. This effect can be neglected by setting $\vartheta = 0$ in (A37).

Assuming quasi equilibrium of the cloud work function we then obtain

$$M_B(i) = -\left(\frac{dA_i}{dt}\right)_{ls} K_{i,i}^{-1} \tag{A39}$$

when the rhs of (A39) is positive, otherwise $M_B(i) = 0$. Here $(dA_i/dt)_{ls}$ is the large-scale forcing of the ith cloud type, which is computed as in (38) of section 2. Once $M_B(i)$ is known, the cumulus-induced changes in θ and q can be calculated as discussed in section 2e.

e. Precipitation formulation

In RAS we assume that all liquid water formed inside a cloud is carried to the top where it is detrained. Then the amount of detrained liquid water $l_{i,i}$ can be computed using (A16). It is then assumed that a fraction of this detrained liquid water is precipitated and the rest is evaporated within the layer of detrainment. We further assume that the precipitation simply falls to the ground without reevaporation in the layers below. Thus, the precipitation R_i for the ith cloud type can be written as

$$R_i = M_B(i)r_i l_{i,i}. \tag{A40}$$

The cloud-type–dependent parameter r_i is chosen as

$$r_i = \begin{cases} 1.0 & p_i < 500 \\ 0.8 + \dfrac{800 - p_i}{1500} & 500 < p_i < 800 \\ 0.8 & p_i > 800, \end{cases} \tag{A41}$$

where p_i is the pressure (hPa) at the detrainment level of the cloud type i.

f. Summary

In summary, the following steps are needed to calculate the cloud-base mass flux and the changes in the temperature and moisture profiles for each cloud type.

1) From the initial profiles of temperature and moisture, compute the dry and moist static energies.
2) Compute the cloud work function for the given cloud type and compute the large-scale forcing [using either (37) or as in LCA].
3) Compute normalized changes of s and h from (A30) and (A31) for the discrete model.
4) Compute the kernel from (A37).
5) Compute the cloud-base mass flux from (A39).
6) Compute the temperature and moisture changes using (A32) and (A33), with the cloud-base mass flux multiplied by the relaxation parameter α.

REFERENCES

Arakawa, A., and W. H. Schubert, 1974: Interaction of cumulus cloud ensemble with the large-scale environment. Part I. *J. Atmos. Sci.*, **31,** 671–701.

——, and M. J. Suarez, 1983: Vertical differencing of the primitive equations in sigma coordinates. *Mon. Wea. Rev.*, **111,** 34–45.

Betts, A., and M. J. Miller, 1986: A new convective adjustment scheme. Part II: Single column tests using GATE wave, BOMEX, ATEX and arctic air-mass data sets. *Quart. J. Roy. Meteor. Soc.*, **112,** 693–709.

Cheng, M. D., and A. Arakawa, 1990: Inclusion of convective downdrafts in the Arakawa–Schubert cumulus parameterization. Tech. Rep. 64 pp. [Available from Department of Atmospheric Sciences, University of California, Los Angeles, CA 90024.]

Chao, W. C., 1979: A study of the conditional instability of the second kind and a numerical simulation of the intertropical convergence zone and easterly waves. Ph.D. dissertation, University of California, Los Angeles, 253 pp.

Cox, S. K., and K. T. Griffith, 1978: Tropospheric radiative divergence during Phase III of GARP Atlantic Tropical Experiment (GATE). Atmos. Sci. Pap. No. 291, Colorado State University, 166 pp.

Hack, J., W. H. Schubert, and P. Silva Dias, 1984: A spectral cumulus parameterization for use in numerical models of the tropical atmosphere. *Mon. Wea. Rev.*, **112,** 704–716.

Kao, C. Y. J., and Y. Ogura, 1987: Response of cumulus clouds to large-scale forcing using the Arakawa–Schubert cumulus parameterization. *J. Atmos. Sci.*, **44,** 2437–2458.

Krishnamurti, T. N., Y. Ramanathan, H. L. Pan, R. J. Pasch, and J. Molinari, 1980: Cumulus parameterization and rainfall rates I. *Mon. Wea. Rev.*, **108,** 465–472.

Lord, S. J., 1978: Development and observational verification of a cumulus cloud parameterization. Ph.D. dissertation, University of California, Los Angeles, 359 pp.

——, 1982: Interaction of a cumulus cloud ensemble with large-scale environment. Part III: Semi-prognostic test of the Arakawa–Schubert cumulus parameterization. *J. Atmos. Sci.*, **39,** 88–103.

——, and A. Arakawa, 1980: Interaction of a cumulus cloud ensemble with large-scale environment, Part II. *J. Atmos. Sci.*, **37,** 2677–2692.

——, W. C. Chao, and A. Arakawa, 1982: Interaction of a cumulus cloud ensemble with large-scale environment. Part IV: The discrete model. *J. Atmos. Sci.*, **39,** 104–113.

Moorthi, S., and A. Arakawa, 1985: Baroclinic instability with cumulus heating. *J. Atmos. Sci.*, **42,** 2007–2031.

Phillips, N. A., 1974: Application of Arakawa's energy conserving layer model to operational numerical weather prediction. Office Note 104, National Meteorological Center, NWS/NOAA, 40 pp.

Ramanathan, Y., 1980: Cumulus parameterization in a case study of a monsoon depression. *Mon. Wea. Rev.*, **108,** 313–321.

Schubert, W. H., 1973: The interaction of a cumulus cloud ensemble with large-scale environment. Ph.D. dissertation, University of California, Los Angeles, 168 pp.

Shukla, J., 1978: CISK–barotropic–baroclinic instability and the growth of monsoon depressions. *J. Atmos. Sci.*, **35,** 495–508.

Silva-Dias, P. L., and W. H. Schubert, 1977: Experiments with a spectral cumulus parameterization theory. Atmos. Sci. Pap. No. 275, Colorado State University, 132 pp.

Sud, Y., and A. Molod, 1988: The roles of dry convection, cloud-radiation feedback processes, and the influence of recent improvements in the parameterization of convection in the GLA GCM. *Mon. Wea. Rev.*, **116,** 2366–2387.

——, W. C. Chao, and G. K. Walker, 1991: Contributions to the implementation of the Arakawa–Schubert cumulus parameterization in the GLA GCM. *J. Atmos. Sci.*, **48,** 1573–1586.

Tiedtke, M., 1989: A comprehensive mass flux scheme for cumulus parameterization in large-scale models. *Mon. Wea. Rev.*, **117,** 1779–1800.

Thompson, R. M., Jr., S. W. Payne, E. E. Recker, and R. J. Reed, 1979: Structure and properties of synoptic-scale wave disturbances in the intertropical convergence zone of the eastern Atlantic. *J. Atmos. Sci.*, **36,** 53–72.

Yanai, M., S. K. Esbensen, and J. H. Chu, 1973: Determination of bulk properties of tropical cloud clusters from large-scale heat and moisture budgets. *J. Atmos. Sci.*, **30,** 611–627.